BACKSTEPPING BOUNDARY CONTROL OF A WAVE PDE WITH SPATIALLY DISTRIBUTED TIME INVARIANT UNKNOWN DISTURBANCES AND ITS APPLICATION TO AN OVERHEAD CRANE MODEL

by

İlhan Umur Ayberk

B.S., Mechanical Engineering, Boğaziçi University, 2015

Submitted to the Institute for Graduate Studies in
Science and Engineering in partial fulfillment of
the requirements for the degree of
Master of Science

Graduate Program in Mechanical Engineering
Boğaziçi University

2018

ACKNOWLEDGEMENTS

I would like to thank my co-advisor Assist. Prof. Halil İbrahim Baştürk for his patient guidance and support in nurturing my academic interests.

I would also like to thank my supervisor Assist. Prof. Evren Samur for his guidance and help he provided when I needed.

I would like to express my thanks to Çetin Yılmaz, and Hakan Yazıcı for participating in my thesis committee.

My friends and colleagues Umut Soysal, Cemal Tuğrul Yılmaz, Erdem Eren, Deniz Irvalı, and Merve Nur Yavuzkaya provided great support, both with their discussions and of course friendship.

Finally, I would like to thank my family for their support and understanding.

ABSTRACT

BACKSTEPPING BOUNDARY CONTROL OF A WAVE PDE WITH SPATIALLY DISTRIBUTED TIME INVARIANT UNKNOWN DISTURBANCES AND ITS APPLICATION TO AN OVERHEAD CRANE MODEL

The aim of this thesis is to control the speed of a payload carried by an overhead crane with the control input provided from the top end of the crane cable. It is assumed that the only measurement available to the controller is from the top end where the cable is attached to the crane car. The motion of the crane model is limited to one horizontal dimension. First, a controller is designed for a simplified mathematical model. The disturbance is assumed to be time invariant, the weight of the crane cable is neglected and the length of the cable is normalized. The exponential stability of this simplified model with the designed controller is proven. Then, the controller is applied to the real crane model with the necessary transformations. Performance of the controller in both cases is shown using numerical simulations in MATLAB. The models are simulated using semi-discretization method for the simplified model and Crank-Nicolson method for the crane model. Perfect reference tracking and disturbance cancellation is achieved under constant disturbances. However, in the presence of time varying effects, the model is stabilized but does not converge perfectly. This result is theoretically expected.

ÖZET

UZAYSAL DAĞILIMLI ZAMANDA DEĞİŞMEZ BİLİNMEYEN BOZULUM İÇEREN DALGA DENKLEMİNİN GERİ ADIMLAMA YÖNTEMİYLE SINIR KONTROLÜ VE TAVAN VİNCİ MODELİNE UYGULANMASI

Bu tezin amacı, bir tavan vinci tarafından taşınmakta olan yükün hızının, tepeden uygulanan kontrol etkisiyle istenen değerde sabitlenmesini sağlamaktır. Kontrolcüde mevcut olan ölçümlerin, yalnızca vinç kablosunun gezici arabaya bağlandığı tepe noktasından alındığı varsayılmıştır. Vinç ve kablonun hareketi, tek bir yatay yönde limitlenmiştir. Öncelikle, basitleştirilmiş bir matematiksel model için kontrolcü tasarlanmıştır. Bu basitleştirimiş modelde, bozucu etkinin zamana göre değişmediği varsayılmış, vinç kablosunun kütlesi ihmal edilmiş ve uzunluğu normalleştirilmiştir. Bu modelin tasarlanan kontrolcü ile üstel olarak kararlı olduğu ispatlanmıştır. Sonrasında, tasarlanan bu kontrolcü, gerekli dönüşümler aracılığıyla, vinç modeline uygulanmıştır. Kontrolcünün iki model üzerindeki performansı, sayısal çözümleme ve benzetim yöntemleriyle incelenmiştir. Basitleştirilmiş modelin benzetiminde yarı-ayrıklaştırma metodu, vinç modeli için ise Crank-Nicolson metodu kullanılmıştır. Sabit bozulum altında referans sinyalinin mükemmel takibi sağlanmıştır. Zamanla değişen bozulum altında model istikrarlı hale gelmiş, fakat mükemmel yakınsama sağlanamamıştır. Bu sonuç teoriyle örtüşmektedir.

TABLE OF CONTENTS

LIST OF FIGURES

LIST OF TABLES

LIST OF SYMBOLS

a	Total disturbance effect
$\hat{a}$	Estimation of the disturbance term a
$\tilde{a}$	Estimation error of a
a_b	Boundary disturbance in the simplified model
a_i	Coefficients of in-domain disturbance in the simplified model
f_g,F	Input horizontal force on the trolley
g	Gravitational acceleration
k	Control gain
l	Crane cable length
m	Mass of the payload
r	Radius of the crane cable
$u(x,t)$	State of the simplified model
u_j^i	Value of the simplified model at i'th time step and j'th spatial node in simulations
$\bar{u}_t(0,t)$	Tracking error of the simplified model
$\hat{\bar{u}}_t(0,t)$	Estimation of the tracking error
$\tilde{\bar{u}}_t(0,t)$	Estimation error of the tracking error
u_t^r	Reference signal for the simplified model
$u_w(y_j,t_i)$	Wind speed at jth spatial node and ith time step
$u_{w,max}(t)$	Maximum wind speed at the given time
$w(y,t)$	Horizontal displacement of each section of the crane cable
$w^c(x,t)$	Target system for the controller
$w^o(x,t)$	Target system for the observer
w_t^r	Reference payload velocity
$y(x,t)$	Measurement delay system
$\hat{y}(x,t)$	Observer system
$\tilde{y}(x,t)$	Observer error system
A,B,C	State space representation matrices

A_c,A_n,B_n,D_n,	
A_p,B_p,D_p	Coefficient matrices and vectors for the numerical simulations
C_D	Drag coefficient
D	Time delay between two ends of the crane rope
$F^j_{drag}(t)$	Drag force on jth section of the crane rope
L	Observer gain vector
M	Mass of the crane trolley
$P(y,t)$	Crane cable tension
P_{eq}	Average crane cable tension
Re	Reynold's number
$U(t)$	Simplified model input
$V(t)$	Lyapunov function
$X(t)$	State space vector of the output boundary
$\hat{X}(t)$	Estimation of the state vector $X(t)$
$\tilde{X}(t)$	observer error of the state vector
$Y(t)$	Signal of the measured states
Δt	Temporal step size
Δy	Spacing between spatial nodes
θ	Crane cable angle for lumped model
$\xi(x,t)$,$\eta(x,t)$,$\zeta(x,t)$	Riemann variables
λ_i	ith eigenvalue of the observer matrix $(A-LC)$
ν	Kinematic viscosity of the fluid medium
$\nu_{cable}(y,t)$	Distributed, time-varying disturbance on the crane cable
$\nu_{load}(t)$	Time-varying disturbance on the payload
ρ	Mass per length of the crane cable
ρ_f	Density of the fluid medium
$\Upsilon(t)$	Norm of the closed loop system errors

LIST OF ACRONYMS/ABBREVIATIONS

1D	One Dimensional
2D	Two Dimensional
3D	Three Dimensional
DoF	Degrees of Freedom
FDM	Finite Difference Method
IDA-PBC	Interconnection and Damping Assignment Passivity-Based Control
LQR	Linear-Quadratic Regulator
LTI	Linear Time Invariant
MoL	Method of Lines
ODE	Ordinary Differential Equation
PDE	Partial Differential Equation
PIDE	Partial Integro-Differential Equation
PSO	Particle Swarm Optimization

1. INTRODUCTION

Cranes are utilized in almost every industry that deals with heavy payloads; port facilities, automobile industry, nuclear power plants and construction sites to name a few. Obviously some of these require high precision and speed in movement and placing of the payload. This might be hard to achieve considering that still in most crane applications, the payload is moved manually by an operator who only has access to visual feedback. The task gets even harder, considering the fact that most of the time the payload ends up in a swinging motion due to the motion of the crane, wind force etc. This swinging motion ends up limiting both the precision and the speed of the operation. Therefore a controller that is capable of rejecting the disturbances on the payload and the crane cable and stabilizing the motion of the payload would greatly benefit both precision and operating speed of such appliances.

1.1. Crane Modeling

The system of interest for this thesis is the overhead crane. An overhead crane consists of a trolley moving on a bridge in one dimension with the cable and the load hanging directly below it an example of which can be seen in Figure 1.1. The up-down motion of the cable relative to the trolley and the back and forth motion of the trolley on the bridge allows 2-DoF control of the payload. In many overhead cranes the bridge itself can move on a third axis which adds up to a 3-DoF motion.

Figure 1.1. A 10 ton overhead crane [1]

Predominantly, there are two approaches followed in modeling an overhead crane system; the lumped-mass model and the distributed-mass model [2].

1.1.1. Lumped-Mass Model

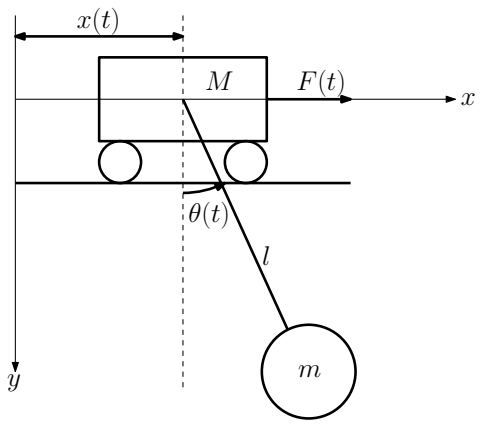

Figure 1.2. Lumped-Mass Crane Model

This model combines the horizontal motion of the trolley with a pendulum-like motion for the crane cable and the payload as seen in Figure 1.2. The equations

of motion for this type of system are found using Lagrange Equations. Kinetic and potential energies of the system are found as

$$T = \frac{1}{2}M\dot{x}^2 + \frac{1}{2}m(\dot{x} + l\dot{\theta})^2 \tag{1.1}$$

$$V = -mgl\cos(\theta) \tag{1.2}$$

$$L = T - V \tag{1.3}$$

Then employing the Lagrange's equations $\frac{d}{dt}\left(\frac{\delta L}{\delta x_i}\right) - \frac{dL}{dx_i} = F_i$, the dynamics of the system are found as

$$(M+m)\ddot{x} + ml\ddot{\theta} = F(t) \tag{1.4}$$

$$\ddot{x} + l\ddot{\theta} + g\theta = 0 \tag{1.5}$$

where M and m are the masses of the trolley and the payload respectively, $F(t)$ is the input force, l is the cable length, $x(t)$ is horizontal position of the trolley, and $\theta(t)$ is the cable angle. There has been numerous control strategies developed using this model. Some of the most occuring ones are discussed below.

Since the model dynamics have a nonlinear nature, some researchers employ linearization strategies. For example, Moustafa and Ebeid [3] develop a nonlinear mathematical model for 2 swing angles of an overhead crane and then linearizes it into the state-space form in order to attenuate the swing motion through feedback control. Later, Park *et al.* [4] develop a nonlinear state feedback controller to regulate vertical and horizontal motion of the payload simultaneously through a novel partial feedback linearization approach.

Some of the studies use adaptive control approaches to account for uncertainties and variations in system parameters. Corriga *et al.* [5] design an adaptive controller to stabilize the swing motion of the load while the cable length is changing. They then use a Lyapunov-like theorem to find an upper bound for the rate of change of cable length such that the crane stays stable with proposed controller. Later, Yang and

Yang [6] achieve perfect gantry position regulation and sway damping while all system parameters are unknown by combining a nonlinear control scheme with an adaptive control law.

Sliding mode approach is often used for this model. Bartolini *et al.* [7] offer a second-order sliding mode based control design for horizontal and vertical motion of the payload. Kuo-Kai Shyu *et al.* [8] offer an anti-swing sliding mode control design in the presence of load mass uncertainty. Then Liu *et al.* [9] combine the sliding mode control with the fuzzy logic approach to design a controller that is capable of adapting to varying system parameters. While the previous attempts relied on linearizations of the crane model Qian *et al.* [10] combine the sliding mode control approach with a fuzzy interface to regulate the control gains without linearizing the model. More recently, Ngo *et al.* [11] improve upon the fuzzy sliding mode control idea by basing the design on the non-linear model of the system.

There are also energy based approaches, to name a few; Aschemann and Schindele [12] propose a passivity-based control scheme where the controller provides adaptive damping to the crane load. They reformulate the system as a Post-Hamiltonian and apply energy-shifting method and IDA-PBC approach. They also apply a nonlinear reduced-order observer to compensate for the nonlinear friction effects. Poljak *et al.* [13] design a nonlinear energy based control structure using the method of Controlled Lagrangians. Sun *et al.* [14] develop a model-free, energy exchanging, dropping-based controller using only the position and swing angle measurements as feedback.

Lastly, there are input/command shaping approaches. Hong *et al.* [15] offer a command shaping control strategy that allows for both horizontal and vertical reference tracking. Then Sorensen *et al.* [16] achieve reference tracking on a 2D horizontal plane by combining position, input shaping, and disturbance rejecting controllers. Recently, Maghsoudi *et al.* [17] improve upon the input shaping control of overhead cranes using PSO algorithm and Ramli *et al.* [18] propose an improved input shaping scheme utilizing an artificial neural network in shaper design where the proposed controller can predict and react to time-varying parameters in the crane system. Abdullahi *et al.*

[19] improve upon previous output-based command shaping designs and propose an adaptive output-based command shaping approach for sway reduction.

1.1.2. Distributed-Mass Model

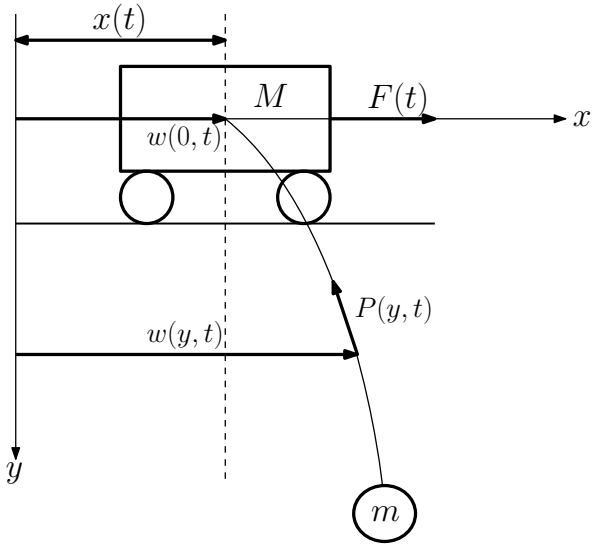

Figure 1.3. Distributed-Mass Crane Model

As can be seen from Figure 1.3, the main difference in this model is that the bending of the cable is considered. The governing equation and the boundary conditions are given as

$$\rho\frac{\delta^2 w(y,t)}{\delta t^2} - \frac{\delta}{\delta y}\left(P(y,t)\frac{\delta w(y,t)}{\delta y}\right) = 0 \tag{1.6}$$

$$M\frac{\delta^2 w(0,t)}{\delta t^2} - P(0,t)\frac{\delta w(0,t)}{\delta y} = F(t) \tag{1.7}$$

$$m\frac{\delta^2 w(l,t)}{\delta t^2} - P(l,t)\frac{\delta w(l,t)}{\delta y} = 0 \tag{1.8}$$

where $w(y,t)$ is the horizontal displacement of the rope at the vertical coordinate y and time t, M and m are the masses of the trolley and the payload, ρ is the mass per unit length of the cable, $F(t)$ is the input force, and $P(y,t)$ is the cable tension calculated as,

$$P(y,t) = mg + \rho g(l-y) \tag{1.9}$$

This model is not studied as extensively as the lumped-mass model. Some of the contributions in this approach are discussed below.

D'Andréa-Novel *et al.* [20] treat the crane system as a PDE-ODE couple. They then implement a class of nonlinear feedback laws to stabilize the gantry position and prove asymptotic stability using La'Salle's Invariance Principle.

Rahn *et al.* [21] use this model to design a boundary control law for asymptotic stabilization of the gantry velocity. They then go on to implement Galerkin's method and root locus analysis to tune control gains in order to dampen out swinging modes of the payload.

Kim and Hong [22] manage to regulate the position of the payload while canceling the swing of the payload. They then achieve stabilization of the sway angle as the payload gets raised or lowered by the hoisting action of the crane cable.

He and Ge [23] design a cooperative boundary control law to stabilize the sway of the payload and minimize the tension in the crane cable through input forces at both trolley and the payload.

1.1.3. Problem Statement

This thesis modifies the aforementioned distributed-mass model slightly with the addition of a spatially distributed time varying disturbance term on the crane cable and a focused time varying disturbance term on the payload. These disturbances can be thought as the drag effect caused by wind or a stream of water for underwater applications. Simple harmonic functions are used to model these arbitrary disturbance effects. The equations of motion given in Equations 1.6 to 1.8 are rewritten with these

modifications

$$\rho w_{tt}(y,t) - \frac{\delta}{\delta y}\left(P(y,t)w_y(y,t)\right) = \nu_{cable}(y,t) \tag{1.10}$$

$$M w_{tt}(0,t) - P(0,t)w_y(0,t) = F(t) \tag{1.11}$$

$$m w_{tt}(l,t) - P(l,t)w_y(l,t) = \nu_{load}(t) \tag{1.12}$$

$$\nu_{cable}(y,t) = A_s(t)u_w(y) \tag{1.13}$$

$$\nu_{load}(t) = A_b \nu_{cable}(l,t) \tag{1.14}$$

where ν_{cable} and ν_{load} are the unknown external effects on the cable and the payload. u_w is the velocity profile of an external fluid flow details of which is discussed in Section 3.2.2 and $A_s(t)$ is the time-varying magnitude of the flow. Lastly A_b is a scaling factor between the payload and the cable signifying the difference in the external force felt by the two due to their difference in shape and size. One can rewrite the governing PDE (Equation 1.10) in its open form,

$$\rho w_{tt} - P_y(y,t)w_y(y,t) - P(y,t)w_{yy}(y,t) = \nu_{cable}(y,t) \tag{1.15}$$

and see that the equation resembles the forced 1D wave equation, which is a second order non-homogeneous hyperbolic PDE of the form

$$w_{tt}(y,t) - c^2 w_{yy}(y,t) = \nu(y,t) \tag{1.16}$$

The only difference between Equation 1.16 and Equation 1.15 is the $P_y(y,t)w_y(y,t)$ term which arises from the change in cable tension along y. The change in the tension is due to the cable's own weight. Therefore, for controller design, $P(y,t)$ is assumed constant on the basis of the cable weight being really small compared to the payload so that the crane system can be represented as a wave equation. The advantage of the wave equation is that there are readily available works on boundary control of the wave equation in the literature which can be used as a stepping stone.

The novelty of this study is that there is no backstepping control method for the wave PDE that can reject both in-domain and boundary disturbances with limited measurement from the input boundary. Similar problems (discussed in Section 1.2) have been solved with full state measurement where all the states $w(y,t)$ are assumed known. Also, there are similar studies where control and measurement are all located at the output boundary. The solution to the problem where the control/measurement and the output are located at opposite boundaries and full state measurement is not available is the contribution of this thesis.

Although this thesis only considers the application of the resulting controller on an overhead crane model, numerous different systems can be represented with or modified into Equation 1.16. Therefore, the controller design can be applied to regulate any system that acts like the forced vibration equation with some simple modifications. A few examples for these applications and some of the previous work on similar topics are given in the next section.

1.2. Method

The stabilization of the wave equation by boundary actuation has been a topic of interest for many years now. Such equations may arise from many physical applications such as oil drilling [24, 25], sea and crane cables [26] and flexible strings [27].

Without an external influence or damping/anti-damping (where the damping coefficient is negative), the wave PDE is a conservative system. The earlier stabilization strategies for such equations are focused on adding a dissipation term to the system so that the overall energy decreases over time. Several methods are developed for the stabilization of wave PDE and they include; spectral methods [28], LQR (linear-quadratic regulator) [29], multiplier technique [30], microlocal analysis [31], Lyapunov functionals [32], and Gramian approach [33] to name a few.

In 2001, a pioneering approach is introduced. In [34], the authors develop the first backstepping control law with infinitely many steps for a first order parabolic PDEs.

For a while this approach was limited to parabolic PDEs. Later, in 2008, [35] applies the backstepping boundary control technique to stabilize an unstable wave PDE. Later, the authors in [36] achieve a methodological breakthrough as they develop a novel integral transformation to stabilize an anti-stable (exponentially stable in negative time) wave PDE with boundary anti-damping and give a backstepping observer design.

Since then, boundary control of the wave equation problem has been expanded in numerous directions. To state a few; the problem of an ODE-PDE cascade where the ODE system is attached to the output boundary of a wave/string PDE is tackled in [37]. In [38], the author proposes the first adaptive controller for anti-stable wave PDE in the case of unmatched parametric uncertainty with the requirement that the entire distributed state of the system is measured. Later, [39] resolves that requirement by introducing Riemann variables.

In more recent works; Bernard and Krstic [40] formulates an adaptive observer for the general 1D hyperbolic PIDEs with unknown system parameters and anti-collocated sensor. Adaptive controller for the 1D wave PDE with anti-collocated, unknown-coefficient, harmonic disturbance is designed in [41]. In [25], a drill string is modelled as a wave PDE and the effect caused by friction is considered as a constant disturbance in the boundary. A boundary controller for the stabilization of the stick-slip oscillations is given for a collocated (sensing and actuation are at the same boundary) case.

However, the topic of in-domain disturbances is fairly unexplored for second order hyperbolic PDEs. In [42] a model-based and a robust adaptive boundary controller for a class of flexible strings with time-varying distributed disturbance are proposed. However, in that study, the actuator, sensor and the state to be controlled are all located at the same boundary. Literature review revealed no study that rejects in-domain disturbances to stabilize one boundary of the wave equation while sensing and control are collocated on the opposite boundary.

In this thesis, an anti-stable wave PDE with time-invariant boundary and in-domain disturbances is considered. The aim is to regulate one boundary of this PDE

with actuation from the opposite boundary. The control is applied as the slope of the input boundary and the sensing is collocated with the control, which, when considered in view of the Riemann variables approach, translates into an LTI system with simultaneous input/output delay.

Then, the controller obtained for the above mentioned anti-stable PDE is applied to the crane model with time-varying disturbances. The simulations are repeated for a couple different disturbance models and references.

At the beginning of Chapter 2, the mathematical model in consideration is examined in detail. The controller design process is given and the closed-loop system stability is proven in the rest of the Chapter 2. Then, the crane model and the necessary transformations are explained in Chapter 3. At the end of both Chapter 2 and Chapter 3, the numerical simulation methods are explained and the simulation results are presented. Results and possible future work are discussed in Chapter 4.

2. CONTROLLER DESIGN FOR THE SIMPLIFIED MODEL

After the model in consideration is explained in detail in Section 2.1, the controller design is handled in three parts. First, the wave equation is reformulated using a technique called Riemann variables in Section 2.2. By expressing the wave equation with Riemann variables, overall behavior of the system can be represented with two separate waves traversing in opposite directions; one traveling from the input boundary to the output boundary and the other from the output boundary back to the input boundary. These two separate waves enable the determination of the states at the output boundary using the measurements at the input boundary with some delay which is considered a delayed measurement of the output boundary.

In Section 2.3, an observer is designed for the delayed measurement and the unknown disturbance effect. The regulator based on this observer is designed in Section 2.4. Sections 2.5 and 2.6 shows the closed-loop system and prove its stability. Lastly, in Section 2.7, the numerical simulations are explained and the results are presented.

2.1. Model

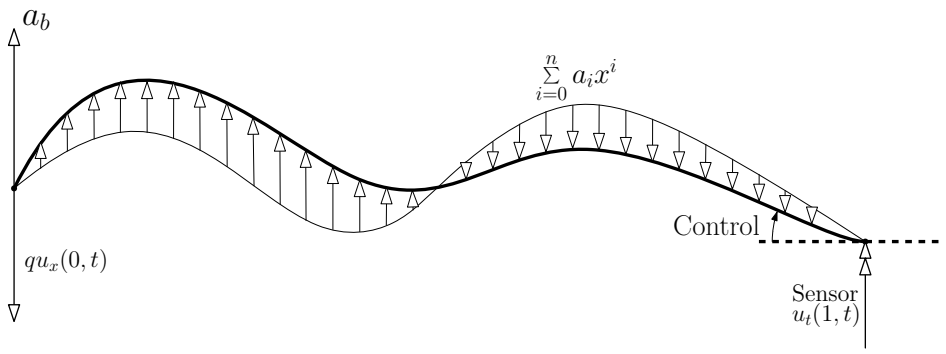

Figure 2.1. Considered wave PDE model

The following wave PDE model is considered

$$u_{tt}(x,t) = u_{xx}(x,t) + \sum_{i=0}^{n} a_i x^i \tag{2.1}$$

with $t > 0$ and spatial coordinate $x \in [0,1]$. The boundary conditions are given by

$$u_x(1,t) = U(t), \tag{2.2}$$

$$u_{tt}(0,t) = -qu_x(0,t) + a_b \tag{2.3}$$

where $U(t) \in \mathbb{R}$ is the input. The constant terms a_i represent the coefficients of in-domain unknown disturbances. The constant unknown disturbance in the boundary is given by a_b. This set of equations can be applied to numerous physical phenomena such as oil drilling [24, 25], sea and crane cables [2], and flexible strings [27]. For the context of this thesis and following the crane example, the in-domain and boundary disturbances may be used to represent a steady external flow (wind, water current etc.) on the crane rope and the load. Boundary term $-qu_x(0,t)$ is the same as the restoring effect of the weight of the payload. The control effort $U(t)$ can be transformed into the force input of the crane with only the measurement of horizontal acceleration of the input boundary.

Following assumptions regarding the plant are made:

Assumption 1. *The plant parameter q is known.*

Assumption 2. *The only available measurements for feedback are the states at $x = 1$.*

By comparing Equation 2.3 and Equation 1.12 in view of Equation 1.9, it can be seen that $q \equiv g$. Assumption 1 is not unrealistic given that the necessary transformations can be applied to the crane system. As for Assumption 2, the states that are

going to be fed back are the angle, velocity and acceleration data from the top end of the cable, which can be done relatively easily via commercially available sensors.

The main aim, for the time being, is to design an adaptive boundary control for $U(t)$ to regulate the rate of change of the state $u_t(0,t)$ at around a desired constant rate u_t^r despite unknown disturbances and limited measurement.

2.2. Reformulation

In this section, the problem stated before is reformulated as a control design for an LTI system in the presence of simultaneous input/output delay and unknown constant disturbance. However since the controller depends on past measurements of the states, first of all two variables; $u_t^p(\tau) = u_t(1,\tau)$ and $u_x^p(\tau) = u_x(1,\tau)$ where $\tau \in [-1, 0]$ are defined. It is assumed that the measurements $u_t^p(\tau)$ and $u_x^p(\tau)$ are available to the controller which assures appropriate behavior at the moment the controller is turned on.

Then, to reformulate the problem, the approach suggested by Bresch-Pietri and Krstic [43] is followed and the following Riemann variables are defined

$$\xi(x,t) = u_t(x,t) + u_x(x,t) \tag{2.4}$$

$$\eta(x,t) = u_t(x,t) - u_x(x,t) \tag{2.5}$$

$$\begin{aligned} z(x,t) =& u_t(1,t+x-1) + u_x(1,t+x-1) \\ =& W(t+x-1) \end{aligned} \tag{2.6}$$

The dynamics of which are given by the transport PDEs,

$$\xi_t(x,t) = \xi_x(x,t) + \sum_{i=0}^{n} a_i x^i \tag{2.7}$$

$$\xi(1,t) = W(t) \tag{2.8}$$

$$z_t(x,t) = z_x(x,t) \tag{2.9}$$

$$z(1,t) = W(t) \tag{2.10}$$

$$\eta_t(x,t) = -\eta_x(x,t) + \sum_{i=0}^{n} a_i x^i \tag{2.11}$$

$$\eta(0,t) = 2u_t(0,t) - \xi(0,t) \tag{2.12}$$

Then solving for $\xi(x,t)$ and $\eta(x,t)$, one gets the following,

$$\xi(x,t) = z(x,t) - \sum_{i=0}^{n} \frac{a_i}{i+1}(x^{i+1} - 1) \tag{2.13}$$

$$\begin{aligned}\eta(x,t) =& 2u_t(0,t-x) - \xi(0,t-x) + \sum_{i=0}^{n} \frac{a_i}{i+1} x^{i+1} \\ =& 2u_t(0,t-x) - z(0,t-x) + \sum_{i=0}^{n} \frac{a_i}{i+1}(x^{i+1} - 1)\end{aligned} \tag{2.14}$$

After this point, the unmeasured state at $x = 0$ is represented in terms of available signals. To this end, from Equation 2.5 and Equation 2.14 the following is derived

$$\eta(1,t) = u_t(1,t) - u_x(1,t) \tag{2.15}$$

$$\eta(1,t) = 2u_t(0,t-1) - \xi(0,t-1) + \sum_{i=0}^{n} \frac{a_i}{i+1} \tag{2.16}$$

Subtracting these two equations from each other and substituting $\xi(0, t-1)$ in view of Equation 2.13 and Equation 2.6, it yields

$$u_t(0, t-1) = \frac{1}{2}\big(u_t(1,t) - u_x(1,t) + u_t(1,t-2) + u_x(1,t-2)\big) \tag{2.17}$$

Equation Equation 2.17 enables expression of the bottom state, delayed by 1 time step, as a function of surface states which are measured. From Equation 2.4, Equation 2.3 is rewritten as follows

$$u_{tt}(0,t) = qu_t(0,t) - q\xi(0,t) + a_b \tag{2.18}$$

Substituting the solution Equation 2.13 yields

$$u_{tt}(0,t) = qu_t(0,t) - qa - qz(0,t) \tag{2.19}$$

where

$$a = \sum_{i=0}^{n} \frac{a_i}{i+1} - \frac{a_b}{q} \tag{2.20}$$

In view of Equation 2.6, it is concluded that $z(0,t) = u_t(1,t-1) + u_x(1,t-1)$ and substituting it into Equation 2.19,

$$u_{tt}(0,t) = qu_t(0,t) - qa - q\left(u_t(1,t-1) + u_x(1,t-1)\right) \tag{2.21}$$

From Equation 2.2, Assumption 2 and Equation 2.17, the system Equation 2.21 can be considered as an ODE with simultaneous input/output delay and a constant unknown disturbance.

2.3. Observer Design

In this section, the observer for both the delayed measurement and the unknown constant disturbance are designed. The aim is to regulate $u_t(0,t)$ at a desired constant value u_t^r.

Adding/subtracting $\pm qu_t^r$ into Equation 2.21,

$$\bar{u}_{tt}(0,t) = q\bar{u}_t(0,t) - qa - q\left(u_t(1,t-1) + u_x(1,t-1) - u_t^r\right) \tag{2.22}$$

where $\bar{u}_t(0,t) = u_t(0,t) - u_t^r$.

Considering Equation 2.17 and noting that a is unknown but constant, the system Equation 2.19 can be written as

$$\dot{X}(t) = AX(t) - Bq\left(u_t(1,t-1) + u_x(1,t-1) - u_t^r\right) \tag{2.23}$$

$$Y(t) = CX(t-1) \tag{2.24}$$

where

$$A = \begin{bmatrix} q & -q \\ 0 & 0 \end{bmatrix}, B = \begin{bmatrix} 1 \\ 0 \end{bmatrix}, C^T = \begin{bmatrix} 1 \\ 0 \end{bmatrix}, X(t) = \begin{bmatrix} \bar{u}_t(0,t) \\ a \end{bmatrix} \tag{2.25}$$

The delayed measurement Equation 2.17 is represented through the following transport PDE,

$$y_t(x,t) = y_x(x,t) \tag{2.26}$$

$$y(1,t) = CX(t) \tag{2.27}$$

$$CX(t-1) = y(0,t) \tag{2.28}$$

Note that the pair (C, A) is observable for $q \neq 0$. The transport PDE representation of the measurement delay allows the use of a backstepping method for the observer design. Following the idea given in [44], the final observer design is as follows,

$$\begin{aligned} \dot{\hat{X}}(t) =& A\hat{X}(t) - Bq\left(u_t(1,t-1) + u_x(1,t-1) - u_t^r\right) \\ &+ e^A L\left(Y(t) - \hat{y}(0,t)\right) \end{aligned} \tag{2.29}$$

$$\hat{y}_t(x,t) = \hat{y}_x(x,t) + Ce^{Ax}L\left(Y(t) - \hat{y}(0,t)\right) \tag{2.30}$$

$$\hat{y}(1,t) = C\hat{X}(t) \tag{2.31}$$

where the observer gain $L \in \mathbb{R}^{2\times 1}$ is chosen so that $(A - LC)$ is Hurwitz and the state

$$\hat{X}(t) = \left[\begin{array}{cc} \hat{\bar{u}}_t(0,t), & \hat{a}(t) \end{array} \right]^T \tag{2.32}$$

represents the estimate of $X(t)$.

The boundedness of the observer error and the convergence are shown in Section 2.6 after designing the controller.

2.4. Observer Based Regulator Design

In this section, a controller for the boundary input $U(t)$ is designed to regulate $u_t(0,t)$ at a desired constant value u_t^r by following the infinite dimensional backstepping technique given by Krstic and Smyshlyaev [44]. The essence of the backstepping procedure is to find an invertible state transformation so that the original systems is transformed to a target system that satisfies the desired properties. Considering Equation 2.19 (or in terms of boundary states as given by Equation 2.21), the following transformation is proposed,

$$\begin{aligned} w^c(x,t) =& z(x,t) - u_t^r + \hat{a}(t) - \left(1 + \frac{k}{q}\right) e^{qx} \hat{\bar{u}}_t(0,t) \\ &+ (q+k) \int_0^x e^{q(x-\tau)} \left(z(\tau,t) - u_t^r + \hat{a}(t)\right) d\tau \end{aligned} \tag{2.33}$$

where $k > 0$.

In Krstic and Smyshlyaev [44], the transformation is given for the case where all states are measured and there is no unknown disturbance. Therefore, by applying the certainty equivalence principle, the unknown states and parameters are substituted by

their estimates that are generated by Equations 2.29 to 2.31.

The control input is derived by setting the boundary $w^c(1,t) = 0$ that allows showing the stability and convergence of the equilibrium of the closed system by a Lyapunov analysis. Substituting $z(x,t)$ given by Equation 2.6, the controller is given by

$$\begin{aligned} U(t) = &- u_t(1,t) + u_t^r - \hat{a}(t) + \left(1 + \frac{k}{q}\right) e^q \hat{\bar{u}}_t(0,t) \\ &- \left(1 + \frac{k}{q}\right) q \int_0^1 e^{q(1-\tau)} \left(u_t(1, t+\tau-1) + u_x(1, t+\tau-1) - u_t^r + \hat{a}(t)\right) d\tau \end{aligned} \tag{2.34}$$

The stability property of the equilibrium of the closed loop system is given in the following theorem.

Theorem 1. *Consider the closed loop system consisting of the plant Equations 2.1 to 2.3, the observer Equations 2.29 to 2.31 and the controller Equation 2.34, and defining*

$$\begin{aligned} \Upsilon(t) = &\left(\bar{u}(0,t) - \hat{\bar{u}}_t(0,t)\right)^2 + \left(a - \hat{a}(t)\right)^2 + \bar{u}_t(0,t)^2 \\ &+ \int_0^1 \left(\left(u_t(x,t) - u_t^r\right)^2 + \left(u_x(x,t) - \hat{a}(t)\right)^2 + \left(y(x,t) - \hat{y}(x,t)\right)^2 \right) dx \end{aligned} \tag{2.35}$$

there exist $\mu > 0$ *and* $\bar{\mu} > 0$ *such that*

$$\Upsilon(t) \leq \mu e^{-\bar{\mu} t} \Upsilon(0) \tag{2.36}$$

Theorem 1 indicates the exponential stability of the equilibrium of the closed loop system in the sense of $\Upsilon(t)^{1/2}$.

The proof of Theorem 1 accomplished by following three main steps. Firstly, the closed loop system represented by transformed states and a target system is obtained. This step allows the second step which consists of proving the exponential stability of the equilibrium of the target system. Lastly, Theorem 1 is proven by applying the inverse transformation and obtaining the stability property in terms of the original states.

The details of the first step is given in the next section.

2.5. Closed-loop System

Firstly, by subtracting Equations 2.23, 2.26 and 2.28 from Equations 2.29 to 2.31, the error system for the observer is obtained

$$\dot{\tilde{X}} = A\tilde{X}(t) - e^{A}L\tilde{y}(0,t) \tag{2.37}$$

$$\tilde{y}_t(x,t) = \tilde{y}_x(x,t) - Ce^{Ax}L\tilde{y}(0,t) \tag{2.38}$$

$$\tilde{y}(1,t) = C\tilde{X}(t) \tag{2.39}$$

where

$$\tilde{y}(x,t) = y(x,t) - \hat{y}(x,t) \tag{2.40}$$

$$\tilde{X}(t) = \left[\widetilde{u}_t(0,t), \quad \widetilde{a}(t)\right] \tag{2.41}$$

with $\widetilde{\bar{u}}_t(0,t) = \bar{u}_t(0,t) - \hat{\bar{u}}_t(0,t)$, $\widetilde{a}(t) = a - \hat{a}(t)$. Employing the same idea which is applied while finding the control input, the infinite dimensional error states $\tilde{y}(x,t)$ are transformed in to a target system. The following transformation

$$w^o(x,t) = \tilde{y}(x,t) - Ce^{A(x-1)}\tilde{X}(t) \tag{2.42}$$

transforms Equations 2.37 to 2.39 into the following target system

$$\dot{\tilde{X}}(t) = \left(A - e^{A}LCe^{-A}\right)\tilde{X}(t) - e^{A}Lw^o(0,t) \tag{2.43}$$

$$w^o_t(x,t) = w^o_x(x,t) \tag{2.44}$$

$$w^o(1,t) = 0 \tag{2.45}$$

Moreover, representing $z(0,t)$ in terms of $w^c(0,t)$ by considering Equation 2.33, substituting it into Equation 2.19, using Equation 2.41 and recalling $\bar{u}_t(0,t) = u(0,t) - u^r_t$, the following dynamics are obtained

$$\bar{u}_{tt}(0,t) = -k\bar{u}_t(0,t) - qw^c(0,t) + [q+k, \ -q]\,\tilde{X}(t) \tag{2.46}$$

Furthermore, the dynamics of transformation Equation 2.42 are given by

$$w^c_t(x,t) = w^c_x(x,t) + [d_u(x), \quad d_a(x)]\,\widetilde{X}(t) + d_{w^o}(x)w^o(0,t) \tag{2.47}$$

$$w^c(1,t) = 0 \tag{2.48}$$

where

$$d_u(x) = (1 + \frac{k}{q})e^{qx}(l_2 - l_1) - \frac{k}{q}e^{-q}l_2 \tag{2.49}$$

$$d_a(x) = (1 + \frac{k}{q})e^{q(x+1)}(l_2 - l_1)(1 - e^{-q}) - \frac{k}{q}(1 - e^{-q})l_2 \tag{2.50}$$

$$d_{w^o}(x) = (1 + \frac{k}{q})e^{q(x+1)}(l_2 - l_1) - \frac{k}{q}l_2 \tag{2.51}$$

The parameters l_1, l_2 are the component of the observer gain defined by $L = \begin{bmatrix} l_1, & l_2 \end{bmatrix}^T$.

At this point, it is important to show the closed-loop system is well-posed before the proving its stability. Using the definition Equation 2.42 and considering the fact that the dynamics given in Equation 2.44 and Equation 2.45 are of a transport PDE, one can see that $w^o(x,t)$ is continuous and converges to zero in finite time. Keeping that in mind and considering that Equation 2.43 is a non-homogeneous first order ODE, by Picard-Lipschitz theorem, it can be concluded that a unique solution exists for $\tilde{X}(t)$ for all $\tilde{X}(0)$. Then the dynamics given by Equation 2.47 and Equation 2.48 can be solved to find the solution of $w^c(x,t)$ as

$$w^c(x,t) = \int_x^1 \left(\begin{bmatrix} d_u(\sigma) & d_a(\sigma) \end{bmatrix} \tilde{X}(t + x - \sigma) + d_{w^o}(\sigma) w^o(t + x - \sigma) \right) d\sigma \tag{2.52}$$

By substituting $x = 0$ in Equation 2.52 one can see that $w^c(0,t)$ is well behaved. Noting that and the previous remark about $\tilde{X}(t)$ and then applying Picard-Lipschitz theorem again, it can be concluded that $\bar{u}_t(0,t)$ also has a unique solution for all $\bar{u}_t(0,0)$. Therefore, finally, it can be concluded that the closed-loop system consisting of Equations 2.42 and 2.48 is well-posed.

To sum up before the stability proof, the plant in consideration is Equations 2.1 to 2.3. The plant is rewritten by using Riemann variables $\xi(x,t)$ and $\eta(x,t)$ given by Equation 2.4. It should be noted that variable $z(x,t)$ is dependent on $\xi(x,t)$ and disturbances as given by Equation 2.13. Therefore, $z(x,t)$ is used instead of $\xi(x,t)$ to

make representation easier. By using the solution of Riemann variables, an expression for $u_t(0, t-1)$ in terms of measured states as given by Equation 2.17 is obtained. An error variable $\bar{u}_t(0,t) = u_t(0,t) - u_t^r$ is defined and unmeasured states $\bar{u}_t(0,t)$ and unknown disturbance a which is the effect of all disturbances on $u_t(0,t)$ are represented by using a vectorial state $X(t)$ given by Equation 2.25. Infinite dimensional part of delayed measurement is denoted by $y(x,t)$. Defining new states $\hat{X}(t), \hat{y}(x,t)$, the observer Equations 2.29 to 2.31 is developed. The observer dynamics firstly written as an error dynamics Equations 2.37 to 2.39 and then the system is transformed in to a target system by using transformation given by Equation 2.42. Thus, observer states are transformed to $\tilde{X}(t), w^o(x,t)$. Similarly, using the transformation Equation 2.33 for mainly $z(x,t)$ the boundary dynamics and $\xi(x,t)$ are transformed to a target system. Thus, $\xi(x,t)$ firstly is represented by $z(x,t)$ and then transformed to $w^c(x,t)$. Finally, the closed loop system is written by the states, $w^c(x,t), w^o(x,t), \eta(x,t), \bar{u}(0,t)_t, \tilde{X}(t)$.

In the next section, the stability of the transformed states are proven. Finally, using the inverse transformation, Theorem 1 is proven.

2.6. Stability

In order to show the stability and convergence of system states and the observers, the following Lyapunov function is defined.

$$\begin{aligned} V = & \int_0^1 (1+x)\left(b_o w^o(x,t)^2 + b_c w^c(x,t)^2\right) dx \\ & + \frac{1}{2}\left(c_c \bar{u}_t(0,t)^2 + c_o \widetilde{X}^T e^{-A^T} P e^{-A} \widetilde{X}\right) \\ & + b_d \int_0^1 e^{1-x}\left(\eta(x,t) - u_t^r + \frac{a_b}{q} - \sum_{i=0}^{n} \frac{a_i}{i+1} x^{i+1}\right)^2 dx \end{aligned} \tag{2.53}$$

where the positive definite matrix P is the solution of

$$(A - LC)^T P + P(A - LC) = -2e^{A^T} Q e^A \tag{2.54}$$

with $Q = Q^T > 0$, $b_d > 0$ and

$$c_c = \frac{1}{k}\left(b_d\left(1 + \frac{k}{q}\right)^2 + 2b\right) \tag{2.55}$$

$$b_c = c_c q^2 \frac{4}{k} + \frac{b_d}{2} + b \tag{2.56}$$

$$c_o = \frac{1}{\lambda_{\min}(Q)}\left(\frac{1}{2} + \frac{4}{k}c_c\Big(\big(q+k\big)^2 + q^2\Big) + 4b_c\Big(\bar{d}_u^2 + \bar{d}_a^2\Big) + \frac{b_d}{2}\Big(\big(1 + \frac{k}{q}\big)^2 + 1\Big) + b\right) \tag{2.57}$$

$$b_o = 4b_c\bar{d}_{w^o} + 2L^T e^{-A} P P e^{-A^T} L + b \tag{2.58}$$

with $b > 0$ and

$$\bar{d}_{w^o} = \max_{x\in[0,1]} |d_{w^o}(x)| \tag{2.59}$$

$$\bar{d}_u = \max_{x\in[0,1]} |d_u(x)| \tag{2.60}$$

$$\bar{d}_a = \max_{x\in[0,1]} |d_a(x)| \tag{2.61}$$

Taking the time derivative of Equation 2.53, noting that

$$\eta(0,t) - u_t^r + \frac{a_b}{q} = \left(1 - \frac{k}{q}\right)\bar{u}_t(0,t) - w^c(0,t) - \left[\left(1 + \frac{k}{q}\right), \quad 1\right]\tilde{X} \tag{2.62}$$

and applying Young's and Cauchy-Schwartz inequalities yield

$$\begin{aligned}
\dot{V} \leq & -b\Bigg[\bar{u}(t)^2 + w^c(0,t)^2 + \int_0^1 w^c(x,t)^2\,dx + w^o(0,t)^2 + \int_0^1 w^o(x,t)^2\,dx \\
& + \widetilde{X}^T(t)\widetilde{X}(t) + \frac{b_d}{2}\left(\eta(1,t) - u_t^r + \frac{a_b}{q} - \sum_{i=0}^{n}\frac{a_i}{i+1}\right)^2 \\
& + \frac{b_d}{2}\int_0^1 e^{(1-x)}\left(\eta(x,t) - u_t^r + \frac{a_b}{q} - \sum_{i=0}^{n}\frac{a_i}{i+1}x^{i+1}\right)^2 dx\Bigg] \\
\leq & -\bar{\mu}V(t)
\end{aligned} \tag{2.63}$$

where $\bar{\mu} > 0$. From Equations 2.53 and 2.63, the following is obtained

$$V(t) \leq e^{-\bar{\mu}t}V(0) \tag{2.64}$$

Considering Equation 2.64, the exponential stability of the equilibrium of the closed loop target system in the sense of transformed states is shown. This result completes the second step of the proof. In the last step, the stability in the sense of original states is shown by performing inverse transformation.

The transformation function Equation 2.33 is written in terms of error states as follows,

$$\begin{aligned} w^c(x,t) =& z(x,t) - u_t^r + a - \left(1+\frac{k}{q}\right) e^{qx}\bar{u}_t(0,t) \\ &+ (q+k)\int_0^x e^{q(x-\tau)}\left(z(\tau,t) - u_t^r + a\right) d\tau \\ &+ \left[\left(1+\frac{k}{q}\right)e^{qx} \qquad \frac{k}{q} - \left(1+\frac{k}{q}\right)e^{qx}\right]\tilde{X}(t) \end{aligned} \tag{2.65}$$

The inverse transformation of Equation 2.33 is given by

$$\begin{aligned} z(x,t) - u_t^r + a =& w^c(x,t) - (q+k)\int_0^x e^{-k(x-\tau)} w^c(\tau,t) d\tau \\ &+ \left(1+\frac{k}{q}\right)e^{-kx}\bar{u}_t(0,t) + \left[-\left(1+\frac{k}{q}\right)e^{-kx} \qquad 1\right]\tilde{X}(t) \end{aligned} \tag{2.66}$$

From Equation 2.42,

$$\tilde{y}(x,t) = w^o(x,t) + Ce^{A(x-1)}\tilde{X}(t) \tag{2.67}$$

Adding Equation 2.4 to Equation 2.5, substituting Equation 2.13, adding and subtracting $\pm\frac{a_b}{2q}$, $\pm u_t^r$ and considering Equation 2.20 yields

$$u_t(x,t) - u_t^r = \frac{1}{2}\left(z(x,t) - u_t^r + a\right) + \frac{1}{2}\left(\eta(x,t) - u_t^r\sum_{i=0}^{n}\frac{a_i}{i+1}x^i + \frac{a_b}{q}\right) \tag{2.68}$$

Similarly, subtracting Equation 2.4 from Equation 2.5, substituting Equation 2.13, adding and subtracting $\pm\frac{a_b}{q}$, $\pm\sum_{i=0}^{n}\frac{a_i}{i+1}x^i$, $\pm\frac{u_t^r}{2}$ and considering Equation 2.20 yields

$$\begin{aligned} u_x(x,t)+\sum_{i=0}^{n}\frac{a_i}{i+1}x^i-\frac{a_b}{q} =&\frac{1}{2}\left(z(x,t)-u_t^r+a\right)\\ &-\frac{1}{2}\left(\eta(x,t)-u_t^r-\sum_{i=0}^{n}\frac{a_i}{i+1}x^i+\frac{a_b}{q}\right) \end{aligned} \tag{2.69}$$

From Equations 2.66 and 2.67, there exist $s_1, s_2, s_3, s_4, s_5 > 0$ such that

$$\|z(x,t)-u_t^r+a\|^2 \leq s_1\|w^c(x,t)\|^2+s_2|\bar{u}_t(0,t)|^2+s_3|\tilde{X}(t)|^2 \tag{2.70}$$

$$\|\tilde{y}(x,t)\|^2 \leq s_4\|w^o(x,t)\|^2+s_5|\tilde{X}(t)|^2 \tag{2.71}$$

From Equations 2.68 and 2.69 and using Equation 2.70, it is shown that there exists $s_6 > 0$ such that

$$\begin{aligned} &\|u_t(x,t)-u_t^r\|^2+\|u_x(x,t)+\sum_{i=0}^{n}\frac{a_i}{i+1}x^i-\frac{a_b}{q}\| \leq\\ &s_6\left(\|w^c(x,t)\|^2+|\bar{u}_t(0,t)|^2+|\tilde{X}(t)|^2+\left\|\eta(x,t)-u_t^r-\sum_{i=0}^{n}\frac{a_i}{i+1}x^i+\frac{a_b}{q}\right\|^2\right) \end{aligned} \tag{2.72}$$

Considering Equations 2.35 and 2.53 and using Equations 2.71 and 2.72, it is shown that

$$\Upsilon(t) \leq \mu_t V(t) \tag{2.73}$$

for some $\mu_t > 0$.

Using Equations 2.4, 2.13 and 2.20, the following expression is obtained

$$z(x,t) - u_t^r + a = (u_t(x,t) - u_t^r) + \left(u_x(x,t) + \sum_{i=0}^{n} \frac{a_i}{i+1} x^i - \frac{a_b}{q}\right) \tag{2.74}$$

From Equations 2.42, 2.65 and 2.74, it is shown that there exist $r_1, r_2, r_3, r_4, r_5, r_6 > 0$ such that

$$\begin{aligned} \|w^c(x,t)\|^2 \leq & r_1 \|u_t(x,t) - u_t^r\|^2 + r_2 \left\| u_x(x,t) + \sum_{i=0}^{n} \frac{a_i}{i+1} x^i - \frac{a_b}{q} \right\| \\ & + r_3 |\bar{u}(t)|^2 + r_4 |\tilde{X}(t)|^2 \end{aligned} \tag{2.75}$$

$$\|w^o(x,t)\|^2 \leq r_5 \|\tilde{y}(x,t)\|^2 + r_6 |\tilde{X}(t)|^2 \tag{2.76}$$

Similarly, considering Equations 2.35 and 2.53 and using Equations 2.75 and 2.76, one can get

$$V(t) \leq \mu_o \Upsilon(t) \tag{2.77}$$

for some $\mu_o > 0$. Thus, Equations 2.64, 2.73 and 2.77 yield Equation 2.36 where $\mu = \mu_o \mu_t$

2.7. Simulations

This section starts off with a detailed explanation of the simulation method in Section 2.7.1. Then in Section 2.7.2, for an example case, chosen model parameters, controller gains, applied disturbances, and the results are presented.

2.7.1. Simulation Method

To simulate this system, a Finite Difference Method (FDM) scheme is developed. Out of multiple categories of FDM schemes, semi-discretization method is chosen. This method is also known as the Method of Lines (MoL) and has been explained in detail previously by Sagert [45].

While the other FDM techniques require discretization on every axis of the domain of a PDE, semi-discretization method calls for discretization of all axes but one. In this case, the PDE is discretized along x but the time derivatives are left as they are. This method has some advantages as it allows different integration techniques or commercial tools that are developed to solve ODEs. For the purposes of this thesis, Euler integration method is used to integrate in time as seen in Equation 2.90.

To formulate this technique, the continuous problem is represented with N uniformly distributed nodal points (t_i, x_j, u_j^i). Then the derivatives in t and x are approximated as

$$\frac{\delta u(x_j, t_i)}{\delta x} = \frac{u_{j+1}^i - u_{j-1}^i}{2\Delta x} \tag{2.78}$$

$$\frac{\delta^2 u(x_j, t_i)}{\delta x^2} = \frac{u_{j+1}^i - 2u_j^i + u_{j-1}^i}{\Delta x^2} \tag{2.79}$$

$$\frac{\delta u(x_j, t_i)}{\delta t} = \frac{du_j^i}{dt} \tag{2.80}$$

$$\frac{\delta^2 u(x_j, t_i)}{\delta t^2} = \frac{d^2 u_j^i}{dt^2} \tag{2.81}$$

Substituting Equations 2.78 to 2.81 into Equation 2.1 gives the discretization of the governing PDE as follows.

$$\frac{d^2u_j^i}{dt^2} = \frac{u_{j+1}^i - 2u_j^i + u_{j-1}^i}{\Delta x^2} + a(x_j) \tag{2.82}$$

where $a(x_j) = \sum a_k x_j^k$.

Following the discretization suggested above, the boundary equations yield what are called ghost nodes that are outside the domain of the system (u_0^i, u_{N+1}^i). For the boundary conditions Equations 2.2 and 2.3, these ghost nodes need to be solved. Rewriting the boundary condition Equations 2.2 and 2.3 in discrete form yields

$$U^i = \frac{u_{N+1}^i - u_{N-1}^i}{2\Delta x} \tag{2.83}$$

$$\frac{d^2u_1^i}{dt^2} = -q\frac{u_2^i - u_0^i}{2\Delta x} + a_b \tag{2.84}$$

where the control input $U^i = U(t_i)$. Solving these for the ghost nodes u_{N+1}^i, u_0^i yields

$$u_{N+1}^i = 2\Delta x U^i + u_{N-1}^i \tag{2.85}$$

$$u_0^i = \left(\frac{d^2u_1^i}{dt^2} - a_b\right)\frac{2\Delta x}{q} + u_2^i \tag{2.86}$$

Plugging these equations into the discretized governing equation Equation 2.82, the dynamics of the boundary nodes are found as

$$\frac{d^2u_N^i}{dt^2} = \frac{2U^i}{\Delta x} + \frac{-2u_N^i + 2u_{N-1}^i}{\Delta x^2} + a(x_N) \tag{2.87}$$

$$\frac{d^2u_1^i}{dt^2}\left(1 - \frac{2}{q\Delta x}\right) = \frac{2u_2^i - 2u_1^i}{\Delta x^2} + a(x_1) - \frac{2}{q\Delta x}a_b \tag{2.88}$$

In the end, for all the nodes in the PDE domain, N linear equations are obtained. These equations are then put into the following matrix form

$$\frac{d\hat{u}^i}{dt} = A_n\hat{u}^i + B_nU^i + D_n \tag{2.89}$$

$$\hat{u}^{i+1} = \hat{u}^i + \frac{d\hat{u}^i}{dt}\Delta t \tag{2.90}$$

where

$$A_n = \left[\begin{array}{ccccc|ccc} 0 & & & & 0 & & & \\ & \ddots & & & & 1 & & 0 \\ & & \ddots & & & & \ddots & \\ & & & \ddots & & & & \\ & & & & \ddots & & & \\ 0 & & & & 0 & 0 & & 1 \\ \hline \frac{-2q}{q\Delta x^2-2\Delta x} & \frac{2q}{q\Delta x^2-2\Delta x} & 0 & \dots & 0 & 0 & & 0 \\ \frac{1}{\Delta x^2} & \frac{-2}{\Delta x^2} & \frac{1}{\Delta x^2} & & \vdots & & \ddots & \\ 0 & \ddots & \ddots & \ddots & 0 & & & \\ \vdots & & \frac{1}{\Delta x^2} & \frac{-2}{\Delta x^2} & \frac{1}{\Delta x^2} & & & \\ 0 & \dots & 0 & \frac{2}{\Delta x^2} & \frac{-2}{\Delta x^2} & 0 & & 0 \end{array}\right] \tag{2.91}$$

$$\hat{u}^i = \begin{bmatrix} u_1 \\ \vdots \\ u_j \\ \vdots \\ u_N \\ \frac{du_1}{dt} \\ \vdots \\ \frac{du_j}{dt} \\ \vdots \\ \frac{du_N}{dt} \end{bmatrix}, \frac{d\hat{u}^i}{dt} = \begin{bmatrix} \frac{du_1}{dt} \\ \vdots \\ \frac{du_j}{dt} \\ \vdots \\ \frac{du_N}{dt} \\ \frac{d^2u_1}{dt^2} \\ \vdots \\ \frac{d^2u_j}{dt^2} \\ \vdots \\ \frac{d^2u_N}{dt^2} \end{bmatrix}, B_n = \begin{bmatrix} 0 \\ \vdots \\ 0 \\ \vdots \\ 0 \\ 0 \\ \vdots \\ \vdots \\ 0 \\ \frac{2}{\Delta x} \end{bmatrix}, D_n = \begin{bmatrix} 0 \\ \vdots \\ 0 \\ \vdots \\ 0 \\ a(x_1) - \frac{2a_b}{q\Delta x} \\ \vdots \\ a(x_j) \\ \vdots \\ a(x_N) \end{bmatrix}$$

2.7.2. Results

10 nodes has been set for the spatial dimension in the simulation. The system parameter q is chosen to be $q = 0.65$. The control gain is chosen as $k = 1$ and the eigen values of the observer matrix $(A - LC)$ are placed at -0.6 and -0.3 resulting in $L = \begin{bmatrix} 1.5500 & -0.2769 \end{bmatrix}^T$.

In the simulation, for $t < 5$, the disturbance is applied to the system and it runs without control input and estimator updates. Then, the proposed controller is applied at $t = 5$ with initial reference $u_r^t = 0$. At $t = 30$ and $t = 55$ marks, the applied disturbance and the reference value are changed in order to see the effect of sudden changes on the closed loop system. Simulation history and the different values of applied disturbance and u_r^t are summarized in Table 2.1.

Table 2.1. Disturbance and reference speed values throughout simulation

time	u_t^r	a_0	a_1	a_2	a_3	a_b	a
$t = 0$	0	-10	20	0	0	1	-1.54
$t = 5$	Controller is turned on						
$t = 30$	3	0	40	-40	0	1.5	4.36
$t = 55$	-5	0	104	-312	208	-2	3.08

The initial disturbance is chosen to be first order in x. At $t = 30$, the disturbance is changed to one that is second order in x and at $t = 55$, a third order disturbance is applied and the boundary disturbance and reference signal u_r^t both change direction and increase magnitude simultaneously. Applied in-domain disturbances can be seen in Figure 2.2.

Figure 2.3 shows the rate of change of $x = 0$ boundary $u_t(0, t)$ and its estimate over time. As can be seen on the figure, the system moves under constant disturbance until $t = 5$ where the controller and estimator update laws are turned on. At about $t = 20$, $u_t(0, t)$ converges to the desired value of 0. At $t = 30$, the first transition can be seen where the second order disturbance is applied and the reference value is changed. Notice the visible effect on the output is due to the sudden shift in a. Lastly,

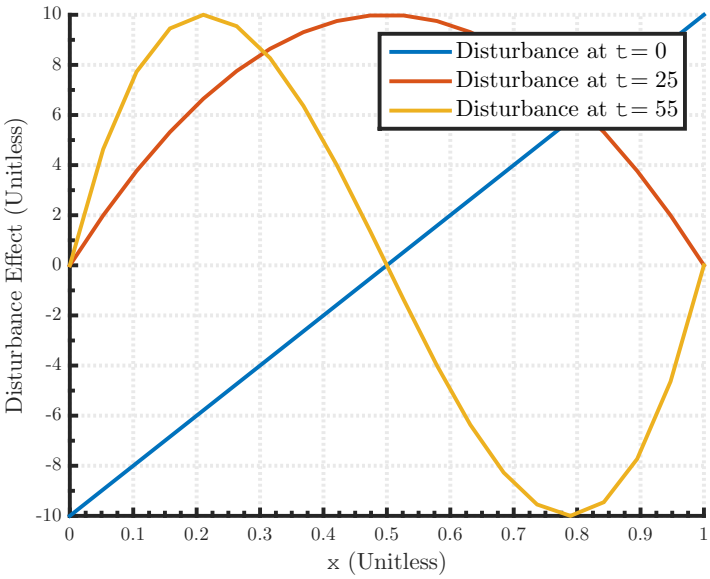

Figure 2.2. Applied in-domain disturbances at different time marks.

at $t = 55$ a milder transition on $u_t(0,t)$ and the estimation can be seen . Although both the boundary disturbance a_b and the reference speed u_t^r change directions at the same time, the change introduced at $t = 30$ has a more visible impact.

It can be seen on Figure 2.4 that perfect estimation of the constant disturbance term a is achieved as predicted in Section 2.6. This concludes the first part of this study where the controller for the normalized target model is designed. As can be seen from the results, exponential convergence of state estimations and tracking error has been accomplished. This is a highly desirable result since the exponential stability is the strongest stability result that can be achieved.

It should be noted that these results are found with constant external effects. In the next chapter, the controller is applied to a crane model where time variant external effects are considered. The reason behind this change is that a constant external effect can almost never be expected in a real life application. It is expected that the controller-observer pair will be able to accommodate slow or small changes in the external effects such that the output will still be marginally stable around the reference value.

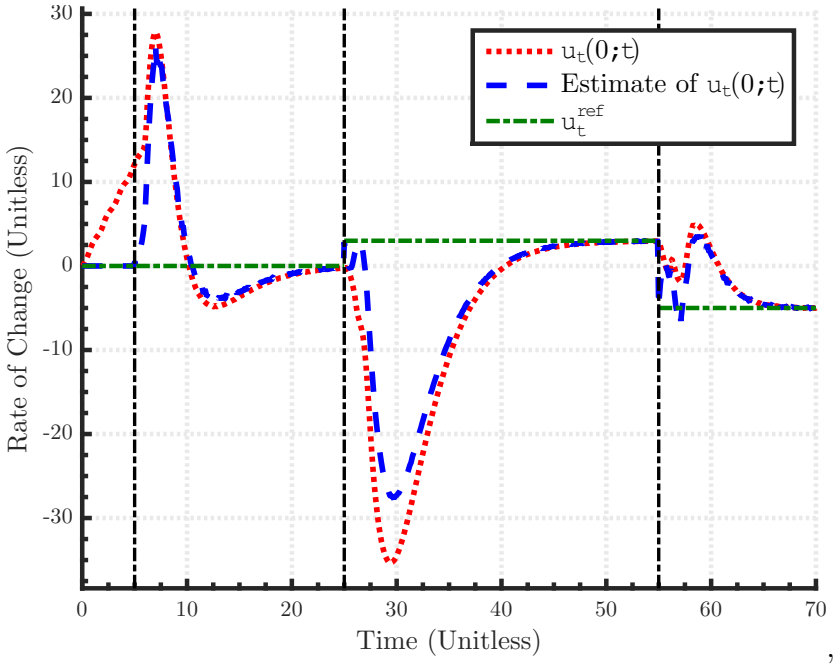

,

Figure 2.3. Resulting speed values of the $x = 0$ boundary and its estimation from numerical simulations.

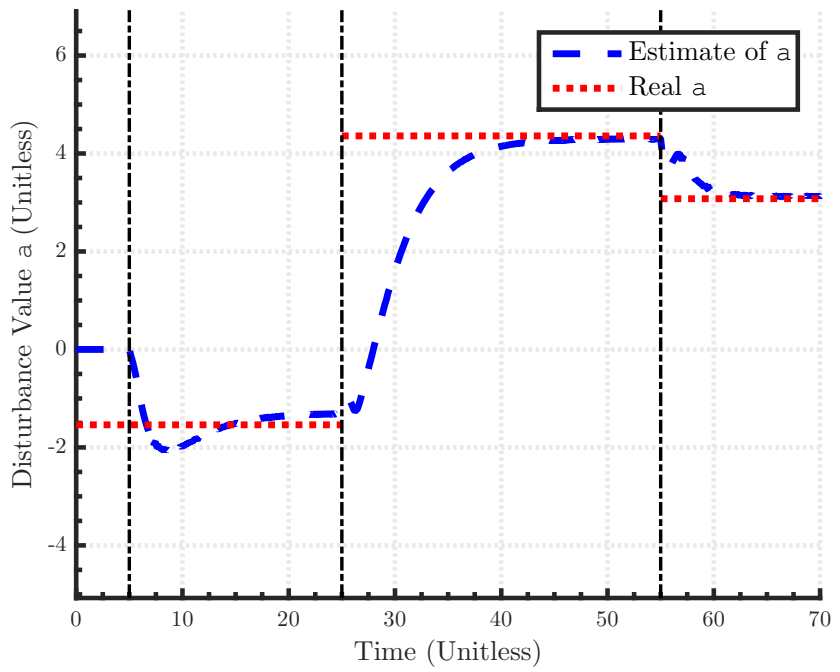

Figure 2.4. The disturbance a and its estimate $\hat{a}(t)$ from numerical simulations.

3. CRANE APPLICATION

A boundary controller that rejects in domain disturbances is designed in the previous section. This section discusses the ways to implement that controller into the overhead crane model. In order to do that, certain transformations have to be made to make the crane model given in Equations 1.10 to 1.12 similar to the wave equation considered for the design of the controller in Equations 2.1 to 2.3. Section 3.1 explains this transformation process and Section 3.3 presents the numerical simulation methods and their results.

3.1. Necessary Transformations

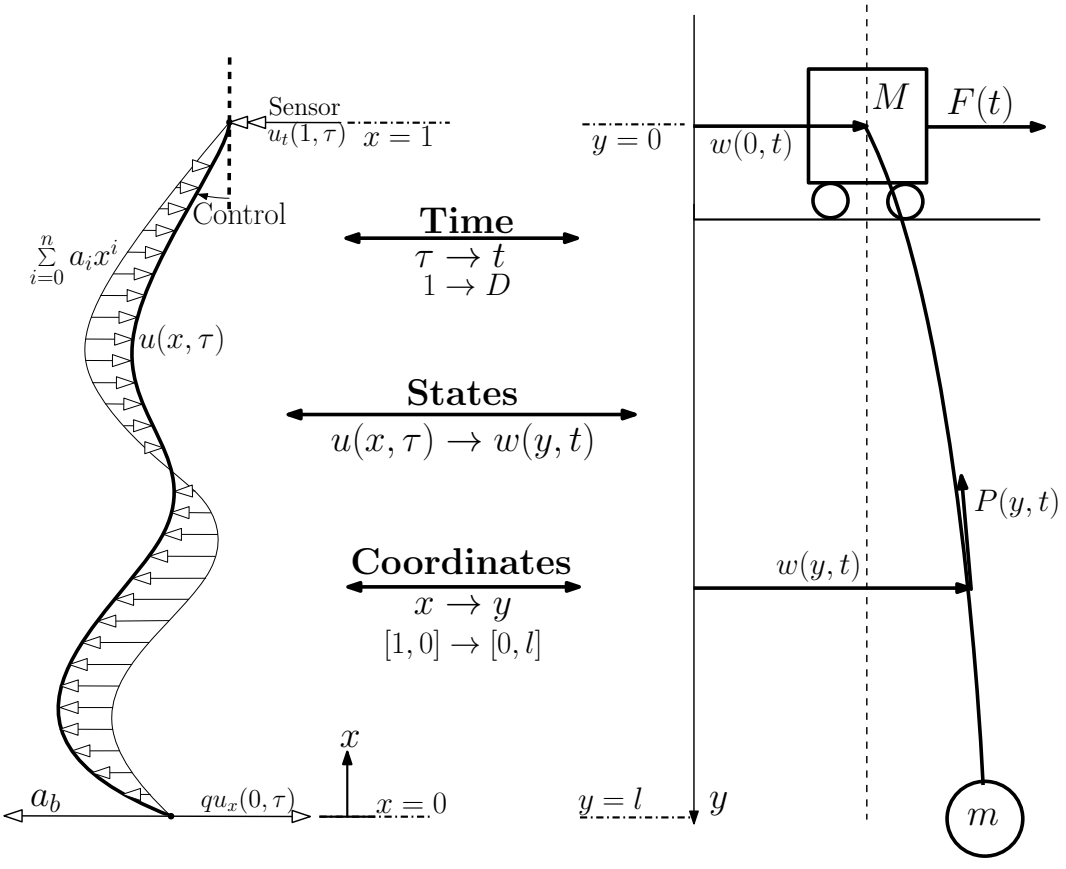

Figure 3.1. Transformation between the controller model and the crane model

Figure 3.1 summarizes the major transformations that are discussed in this section. First off, the governing equations need to be transformed into each other. The

equations in consideration are

$$u_{\tau\tau}(x,\tau) - u_{xx}(x,\tau) = \nu_u(x,\tau) \tag{3.1}$$

$$\rho w_{tt}(y,t) - P_{eq} w_{yy}(y,t) = \nu_{cable}(y,t) \tag{3.2}$$

Notice there are a couple of changes to both the crane model PDE and the controller model PDE. First, the temporal term of the first equation τ is introduced which is needed since the wave speed and domain lengths are different between two systems and the aim is to equate the delay time of the crane model to the unit delay considered in the controller. Also the disturbance term in the crane model is assumed constant for the time being. Lastly, the equivalent tension term P_{eq} is introduced which is calculated as $P_{eq} = \frac{P(0)+P(l)}{2}$. Since the wave speed on the cable depends on this $P(y)$ term, P_{eq} is chosen as its average to be able to calculate the real delay time for the crane system.

Since the controller is placed at $x = 1$ on the first system and the control input of the crane model is at $y = 0$ and the outputs are located at $x = 0$ and $y = l$, the transformation between spatial coordinates x and y need to map $(1, 0) \to (0, l)$. Then the following transformation is suggested.

$$y = (1 - x)l \tag{3.3}$$

The next goal is to equate the temporal terms of both systems. Since the wave speed in the crane PDE is calculated as $\sqrt{\frac{P_{eq}}{\rho}}$, the delay in the crane system is $D = \sqrt{\frac{\rho}{P_{eq}}}l$. The delay time in the first system was 1, so the transformation needs to equate 1 unit time passed in τ to D seconds in t. Then the following transformation is applied.

$$t = \sqrt{\frac{\rho}{P_{eq}}}l\tau \tag{3.4}$$

In view of Equations 3.3 and 3.4, one can rewrite $u(x,\tau)$ and $w(y,t)$ as,

$$u(x,\tau) = w(l(1-x), D\tau) \tag{3.5}$$

Then the spatial and temporal derivatives are related as

$$u_\tau(x,\tau) = Dw_t(y,t) \tag{3.6}$$
$$u_{\tau\tau}(x,\tau) = D^2 w_{tt}(y,t) \tag{3.7}$$
$$u_x(x,\tau) = -lw_y(y,t) \tag{3.8}$$
$$u_{xx}(x,\tau) = l^2 w_{yy}(y,t) \tag{3.9}$$

Substituting Equations 3.6 to 3.9 into the boundary equations, the rest of parameters and terms are transformed using the following equations.

$$u_\tau^r = Dw_t^r \tag{3.10}$$
$$q = -\frac{P(l)D^2}{ml} \tag{3.11}$$
$$\frac{\nu_{b,u}(\tau)}{D^2} = \frac{\nu_{payload}(t)}{m} \tag{3.12}$$
$$F(t) = \frac{P}{l}U(\tau) + Mw_{tt}(0,t) \tag{3.13}$$
$$\frac{\nu_u(x,\tau)}{D^2} = \frac{\nu_{cable}(y,t)}{\rho} \tag{3.14}$$

Now that all the required parameters and variables can be transformed back and forth between controller and crane model, the control strategy is to take the measurements $w(0,t), w_t(0,t), w_{tt}(0,t)$, and $w_y(0,t)$ then transform them into their equivalents $u(1,\tau), u_\tau(1,\tau), u_{\tau\tau}(1,\tau)$, and $u_x(1,\tau)$. Then calculate $U(\tau)$ using the transformed measurements and the observer and regulator designs given in Chapter 2 and, lastly, transform the control input $U(\tau)$ back into the trolley force $F(t)$.

3.2. Disturbance Model

In terms of disturbances and external effects on the system, two cases are considered in the simulations where all the effects are assumed to be the product of an external fluid flow field. First, just a spatially distributed time varying disturbance model is applied to the cable. In that case, external force on the payload is considered equal to the in-domain disturbance at $y = l$ position.

In the second case, payload force is increased by a factor of the in-domain disturbance at the same position. This scaling corresponds to the rope and the payload being subjected to the same flow but experience different forces due to their difference in shape and size.

For the last case, drag effect is considered. Drag force on different sections of the rope is roughly approximated, again to keep the computational difficulty at a reasonable level.

3.2.1. Drag Force Approximation

Any object immersed in a fluid field that is in relative motion to the object will experience drag force. Drag is the net force along flow direction [46] and it is calculated for each section of the cable (see Figure 3.2) using the following formula.

$$F^j_{drag} = \frac{1}{2} C_d \rho_f \pi r u^2_w(y_j, t_i) dy \tag{3.15}$$

where, C_d is the drag coefficient of the cable, ρ_f is the density of the fluid, r is the cable radius and $u(y^j, t)$ is the horizontal velocity of the jth node on the cable. The cable radius is chosen to be 4 mm which is the same as some commercially available crane cables on the thin end. The density values used are 1.225 kg/m^3 for air and 997 kg/m^3 for water. Generally speaking, the value of C_d depends on geometrical shape, surface type of the object and the Reynold's number for the flow.

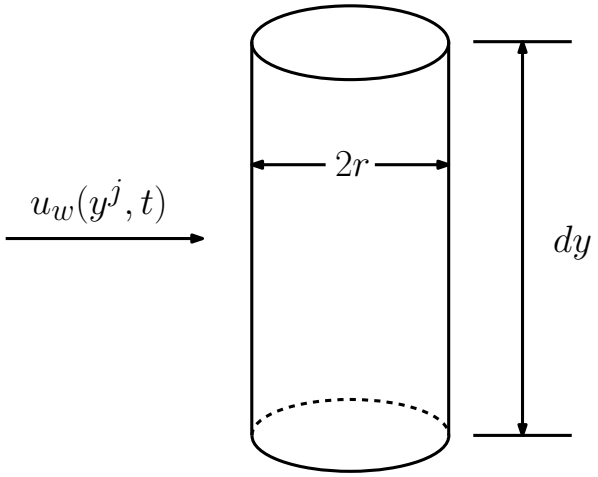

Figure 3.2. Cylindrical cable section subject to the flow field $u_w(y, t)$

A couple assumptions are made when approximating the drag force. First, the cable is assumed straight at all times, meaning any rotation is neglected and each section of the cable is assumed to be vertical. Following the first assumption, all the motion is assumed to be on the horizontal axis. Lastly, the Reynold's number and therefore the drag coefficient are assumed constant throughout the simulation for ease of calculation.

As mentioned above, the drag coefficient depends on Reynold's number and it is defined as follows

$$R_e = \frac{vl}{\nu} \tag{3.16}$$

where v is the relative flow speed, l is a significant length of the object, and ν is the kinematic viscosity of the fluid. In this case, value for l is chosen to be the cable diameter. A typical speed of $v = 3$ m/s is used since it is the example reference velocity chosen for the simulations as well. The kinematic viscosity values for air and water are 1.48×10^{-5} m^2/s and 1 m^2/s respectively. Substituting the values into Equation 3.16, $Re = 2.7 \times 10^3$ is found for air and $Re = 0.04$ is found for water.

Using the data given by Naval Civil Engineering Laboratory [47], drag coefficient in the case of air as the medium is chosen to be $c_D = 1.2$ which is an average value for a couple different steel cables with similar Reynold's number values. For the case with water as the medium, a value of $C_D = 3$ is chosen using a data set for smooth cylinders in cross flow given by Munson *et al.* [46].

3.2.2. In-Domain and Boundary Disturbances

Following the assumptions and simplifications stated previously in Section 3.2.1 and Equation 3.15 , one can argue that any external force caused by the fluid flow around the crane system is proportional to the flow speed at each section along the cable and the payload. That is to say, since the cable is assumed uniform and relatively straight at all times, each cross section has the same drag coefficient C_d, same radius r, and is exposed to the same fluid density ρ_f, then following Equation 3.15, the disturbing force distribution is just the flow speed distribution squared in magnitude and scaled by a factor $C_d \rho_f \pi r$.

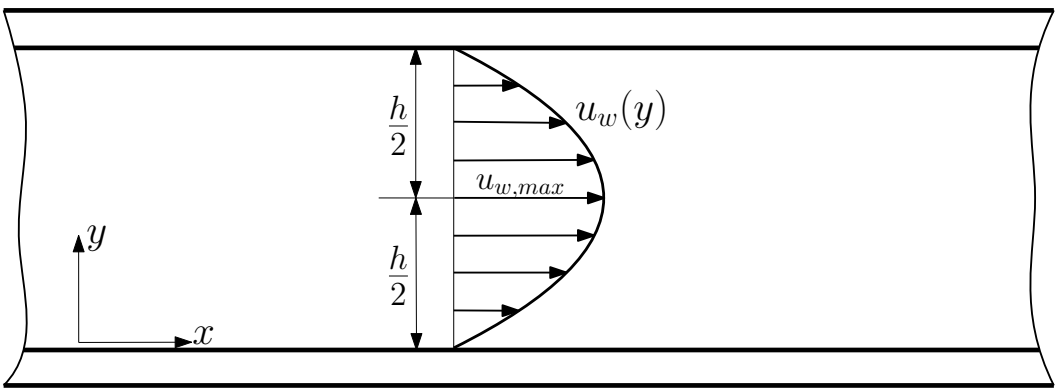

Figure 3.3. Viscous flow between two parallel plates

One simple flow speed distribution is chosen for the simulations. This flow profile arises from viscous fluid flow between infinitely long parallel plates as illustrated in Figure 3.3. This example is chosen because it has a simple polynomial solution and for any in-door operation, the ceiling and the floor can be thought of as parallel plates.

The solution for this problem is given by Munson *et al.* [46] as

$$u_w(y) = \frac{1}{2\mu}\frac{\delta p}{\delta x}y^2 + c_1 y + c_2 \tag{3.17}$$

where $\frac{\delta p}{\delta x}$ is the pressure gradient and considered constant and the constants c_1, c_2 are to be determined by imposing the boundary condition that the flow speed is zero where the fluid touches the plates. Since the flow speed is zero at the boundaries, Equation 3.17 can be rewritten as follows,

$$u_w(y) = \frac{1}{2\mu}\frac{\delta p}{\delta x}(y - c_1')(y - c_2') \tag{3.18}$$

where c_1' and c_2' are the y positions of the top and bottom plate or the ceiling and the floor of the working area. Due to the no-slip condition on ceiling and the floor, the flow speed will always be zero at those points. Therefore if the payload is placed at the bottom of the work area, the boundary disturbance of the crane system will be zero at all times. To prevent that, the work area height h is introduced and the trolley or the top boundary of the crane is assumed to be on the ceiling. Then, substituting $c_1' = 0$ and $c_2' = h$ as the boundaries, the flow profile becomes

$$u_w(y) = \frac{1}{2\mu}\frac{\delta p}{\delta x}(y^2 - hy) \tag{3.19}$$

It can easily be seen that the extremum value of the flow velocity is at the middle $u_{w,max} = u_w(\frac{h}{2}) = -\frac{1}{2\mu}\frac{\delta p}{\delta x}\frac{h^2}{4}$. For the ease of scalability later in the runtime it is desirable to have a flow shape with its peak value at $u_{w,max} = 1$ so the polynomial is normalized with a factor of $-\frac{4}{h^2}$ and the rest of the terms are grouped in to a single time-varying parameter which can be used to set the maximum flow speed to any desired value during simulation. Resulting flow profile is shown in Figure 3.4 for which an exact mathematical expression is given in Equation 3.20. Notice that the region of interest for the flow profile is only $y \in [0, l]$ for the purposes of the crane system.

$$u_w(y,t) = u_{w,max}(t)(-\frac{4}{h^2})(y^2 - hy) \tag{3.20}$$

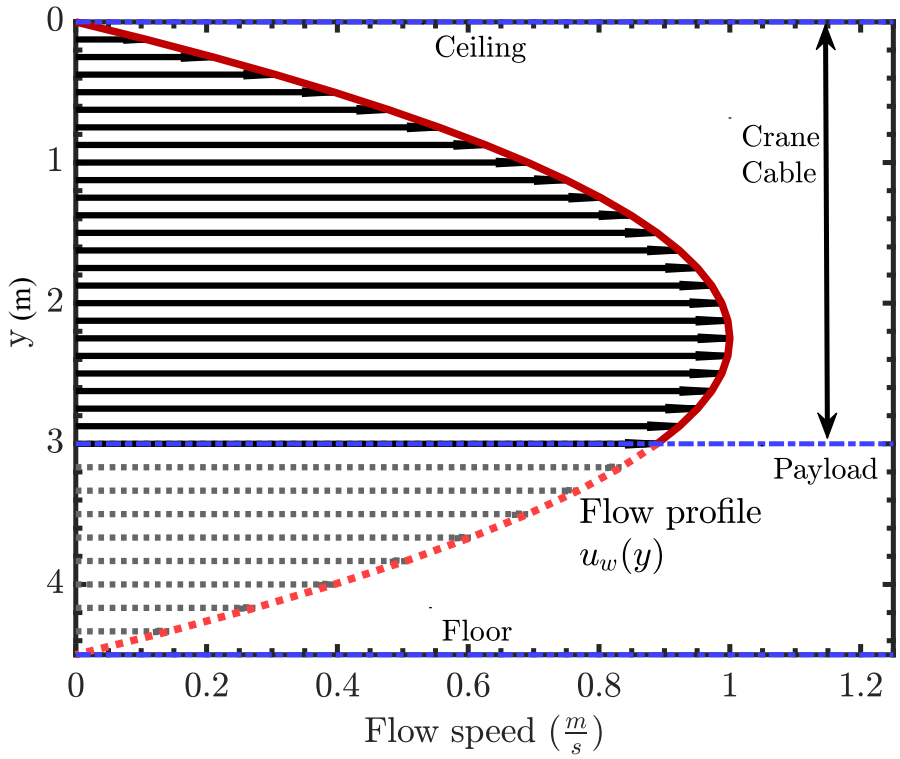

Figure 3.4. Flow speed distribution $u_w(y)$ direction with $u_{max} = 1$ m/s

3.3. Simulations

This section first explains the method with which the real crane system is simulated, then the results for an example case with a couple different disturbance types is given.

3.3.1. Simulation Method

Unlike the first set of simulations in Section 2.7, a Crank-Nicolson scheme is applied for the crane system. Crank-Nicolson method is known to be unconditionally stable for diffusion or wave type PDEs [48]. This is done to ensure numerical stability as the system parameters and the variables get larger in magnitude with respect to the relatively small scale simulations that were done previously.

Crank-Nicholson method calls for discretization of both spatial and temporal dimensions. The derivative approximations are done in what is called a "middle step" between two discrete temporal nodes. As the derivatives are approximated in that middle step, the governing equation includes past and future states of the same spatial node. Then, by representing the governing discretized equation in matrix form, the future states are solved for using inverse matrices. Therefore, first, the following approximations are defined,

$$w_{tt}(y_j, t_i) = \frac{w_j^{i-1} - 2w_j^i + w_j^{i+1}}{\Delta t^2} \tag{3.21}$$

$$w_y(y_j, t_i) = \frac{1}{4\Delta y}\left(w_{j+1}^{i+1} - w_{j-1}^{i+1} + w_{j+1}^{i-1} - w_{j-1}^{i-1}\right) \tag{3.22}$$

$$w_{yy}(y_j, t_i) = \frac{1}{2\Delta y^2}\left(w_{j+1}^{i+1} - 2w_j^{i+1} + w_{j-1}^{i+1} + w_{j+1}^{i-1} - 2w_j^{i-1} + w_{j-1}^{i-1}\right) \tag{3.23}$$

Then, substituting into Equation 1.10, the governing equation is discretized as follows,

$$\begin{aligned} w_j^{i+1}(1 + 2\lambda_j) + w_{j+1}^{i+1}(-K - \lambda_j) + w_{j-1}^{i+1}(K - \lambda_j) = 2w_j^i + \nu(y_j, t_i)\Delta t^2 \\ + w_{j+1}^{i-1}(K + \lambda_j) + w_{j-1}^{i-1}(-K + \lambda_j) + w_j^{i-1}(-1 - 2\lambda_j) \end{aligned} \tag{3.24}$$

where,

$$\lambda_j = \frac{P(y_j)\Delta t^2}{2\rho\Delta y^2} \tag{3.25}$$

$$K = \frac{-9\Delta t^2}{4\Delta y} \tag{3.26}$$

Then substituting Equations 3.21 to 3.23 into the boundary conditions Equations 1.11 and 1.12 and solving for ghost nodes as described in Section 2.7.1, discretized

boundary equations are found as

$$w_1^{i+1}(1+2\lambda_1-K_1(-K+\lambda_1))+w_2^{i+1}(-2\lambda_1)=w_1^i(2-2K_1(-K+\lambda_1))$$
$$+w_1^{i-1}(-1-2\lambda_1+K_1(-K+\lambda_1))+w_2^{i-1}(2\lambda_1)$$
$$+f_g(t_i)(K_2(-K+\lambda_1))+\nu(y_1,t_i)(\Delta t^2+K_2(-K+\lambda_1)) \tag{3.27}$$

where,

$$K_1=\frac{-4M\Delta y}{P(y_1)\Delta t^2} \tag{3.28}$$
$$K_2=\frac{4\Delta y}{P(y_1)} \tag{3.29}$$

and

$$w_N^{i+1}(1+2\lambda_N-K_3(K+\lambda_N))+w_{N-1}^{i+1}(-2\lambda_N)=w_N^i(2-2K_3(K+\lambda_N))$$
$$+w_N^{i-1}(-1-2\lambda_N+K_3(K+\lambda_N))+w_{N-1}^{i-1}(2\lambda_N)+\nu(y_N,t_i) \tag{3.30}$$

where,

$$K_3=\frac{-4m\Delta y}{P(y_N)\Delta t^2} \tag{3.31}$$
$$K_4=\frac{4\Delta y}{P(y_N)} \tag{3.32}$$

Following these steps, N linear difference equations are obtained. Then these equations are expressed in matrix form,

$$A_n\hat{w}^{i+1}=A_p\hat{w}^{i-1}+A_c\hat{w}^i+B_cf_g(t_i)+D_c(t_i) \tag{3.33}$$

where,

$$A_n = \begin{bmatrix} 1+2\lambda_1 - K_1(-K+\lambda_1) & -2\lambda_1 & & 0 \\ \ddots & \ddots & \ddots & \\ & (K-\lambda_j) & (1+2\lambda_j) & (-K-\lambda_j) \\ & \ddots & \ddots & \ddots \\ 0 & & -2\lambda_N & 1+2\lambda_N - K_3(K+\lambda_N) \end{bmatrix} \tag{3.34}$$

$$A_p = \begin{bmatrix} -1-2\lambda_1 + K_1(-K+\lambda_1) & 2\lambda_1 & & 0 \\ \ddots & \ddots & \ddots & \\ & (K+\lambda_j) & (-1-2\lambda_j) & (-K+\lambda_j) \\ & \ddots & \ddots & \ddots \\ 0 & & 2\lambda_N & -1-2\lambda_N + K_3(K+\lambda_N) \end{bmatrix} \tag{3.35}$$

$$A_c = \begin{bmatrix} 2-2K_1(-K+\lambda_1) & & & 0 \\ & 2 & & \\ & & \ddots & \\ & & 2 & \\ 0 & & & 2-2K_3(K+\lambda_N) \end{bmatrix} \tag{3.36}$$

$$\hat{w}^i = \begin{bmatrix} w(y_1,t_i) \\ \vdots \\ w(y_j,t_i) \\ \vdots \\ w(y_N,t_i) \end{bmatrix}, B_c = \begin{bmatrix} K_2(-K+\lambda_1) \\ 0 \\ \vdots \\ \vdots \\ 0 \end{bmatrix}, D_c(t_i) = \begin{bmatrix} \nu(y_1,t_i) \\ \vdots \\ \nu(y_j,t_i) \\ \vdots \\ \nu(y_N,t_i) \end{bmatrix} \tag{3.37}$$

Then, at each time step, the values of $w(y,t)$ in the next time step $w(y_j, t_{i+1})$ are calculated using,

$$\hat{w}^{i+1} = A_n^{-1}A_c\hat{w}^i + A_n^{-1}A_p\hat{w}^{i-1} + A_n^{-1}B_c f_g(t_i) + A_n^{-1}D_c(t_i) \tag{3.38}$$

3.3.2. Results

5 nodes are set along y direction. The crane parameters are chosen as follows; mass of the trolley $M = 75$ kg, mass of the payload $m = 1500$ kg, nominal length mass of the cable $\rho = 6$ kg/m, and the cable length $l = 3$ m. The control parameters are chosen as the control gain $k = 0.05$ and the eigenvalues of the observer system $A - LC$, $\lambda_1 = -0.0550$, $\lambda_2 = -0.0275$. The reason for such low controller parameters is again the overall numbers getting larger as the scale gets larger. Although the numerical solution of the open-loop PDE is unconditionally stable, the closed-loop system may become numerically unstable with higher controller or observer gains in which case the simulations have to be done with much smaller time steps and that would increase the computational cost.

The system is simulated for 75 seconds. For the first 35 seconds of the simulation, the reference payload velocity is set to be $w_t^r = 3$ m/s. Then at $t = 35$, the reference velocity is set to $w_t^r = 0$.

Several types of external conditions are applied to the system in simulations. The variables are in-domain disturbance, boundary disturbance, drag caused by the cable's own motion, and the fluid medium. The controller is tested against several combinations of these and two cases with constant flow speed are shown as a proof of the controller's performance in canceling constant disturbances. Values of all parameters except the fluid properties are the same for each case, the effects are just activated or inactivated depending on the case studied. Following subsections cover each case separately. Please note that the *drag* referred to in case titles is meant as the drag force in response to the system's motion not the drag caused by external flow. In-domain

and boundary disturbances are still calculated through the drag caused by fluid flow.

(i) *Case 0: Open-loop simulation :* Before testing the controller, an open-loop simulation is shown in this section for comparison. In this case, the medium is chosen as air and the wind distribution has the shape shown in Figure 3.6 but the maximum wind speed function is chosen to have no bias term but have the same sinusoidal component as other cases. The resulting maximum wind speed is found as

$$u_{w,max}(t) = 5\sin(0.05\pi t) \tag{3.39}$$

This disturbance model is chosen so that the swaying motion caused by the harmonic disturbance can be seen more clearly. Also, the drag effect caused by the crane motion is considered. It can be seen in Figure 3.5 that time varying disturbance causes up to 0.78 m/s deviation from the 0 m/s line with no control input.

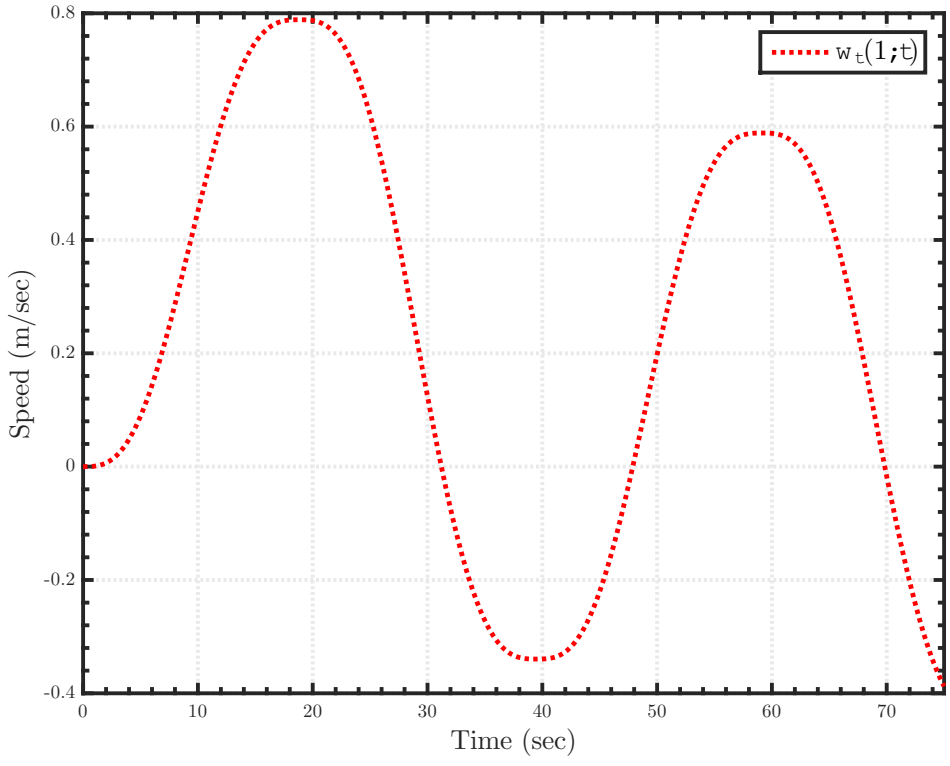

Figure 3.5. Horizontal velocity of the payload and its estimation for Case 0

(ii) *Case 1: Time varying in-domain disturbance without boundary disturbance or drag (air) :*

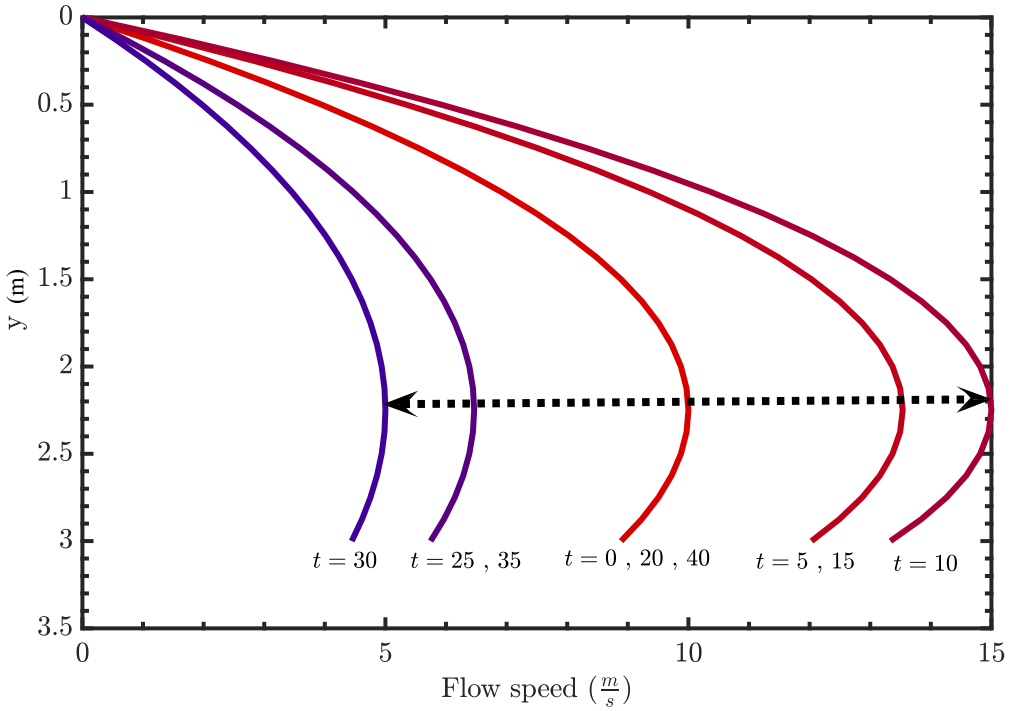

Figure 3.6. Time progression of the flow speed distribution

In this case, the system is subject only to an external airflow. The disturbance scaling (discussed in Section 3.2) at the payload boundary is not considered. Time varying air flow is calculated using Equation 3.20 with the maximum wind speed at any given time $u_{w,max}(t)$ is chosen as follows.

$$u_{w,max}(t) = 10 + 5\sin(0.05\pi t) \tag{3.40}$$

The resulting wind speed distribution has a time varying maximum wind speed that oscillates between $5 - 15$ m/s and has a period of 40 s. This average wind speed of 10 m/s is placed at the higher end of a *Fresh Breeze*, close to a *Strong Breeze* by Beaufort Scale [49]. The exact value of the wind speed at each section in a given time step t_i is calculated as follows and the distribution at several time

points are shown in Figure 3.6.

$$u_w(y_j, t_i) = \frac{4y_j(y_j - l)}{l^2}\left(10 + 5\sin(0.05\pi t_i)\right) \tag{3.41}$$

Figures 3.7 to 3.9 show the resulting payload velocity $w_t(1,t)$, disturbance $a(t)$, and the input force $f_g(t)$ values versus time. It can be seen on Figure 3.7 that convergence to the reference velocity is achieved almost perfectly. There is an oscillatory period initially when the system is just turned on or when the reference velocity is changed. However that behavior depends heavily on the control/observer gain values for the given case. It has been seen in other simulations that the payload velocity can act like an over-damped or critically-damped system depending on external effects and the gain values. Such examples can be seen in Cases 7 and 8.

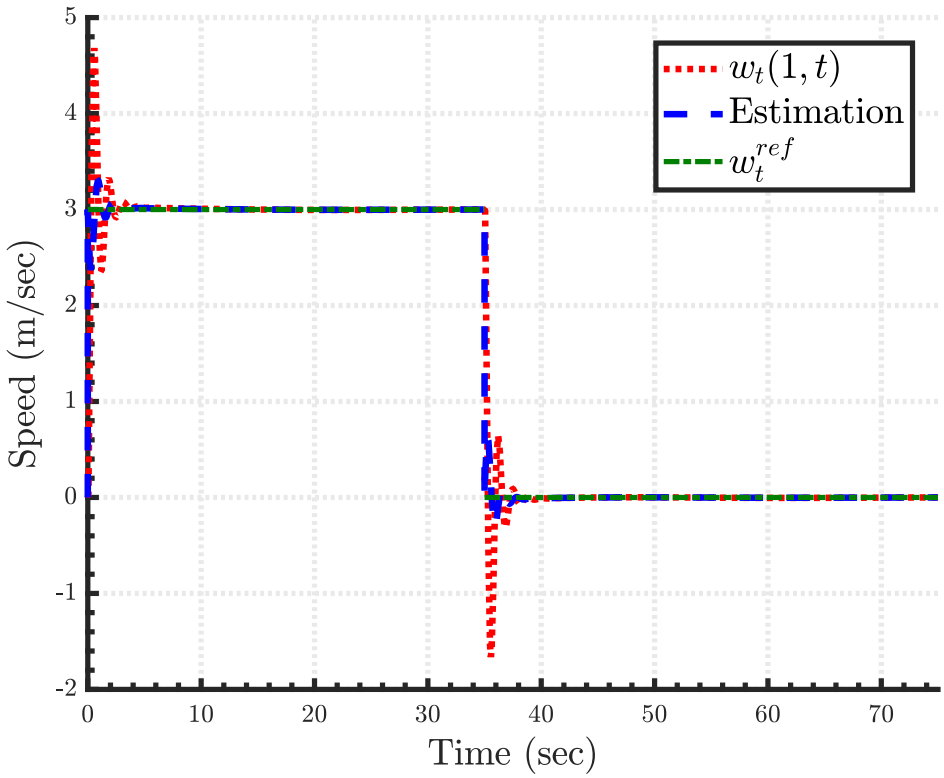

Figure 3.7. Horizontal velocity of the payload and its estimation for Case 1

It can be seen on Figure 3.8 that the estimation of the disturbance effect is achieved relatively successfully. There seems to be a phase shift between the estimation signal $\hat{a}(t)$ and the disturbance signal $a(t)$ which is expected as the

observer design assumes the disturbance effect to be constant.

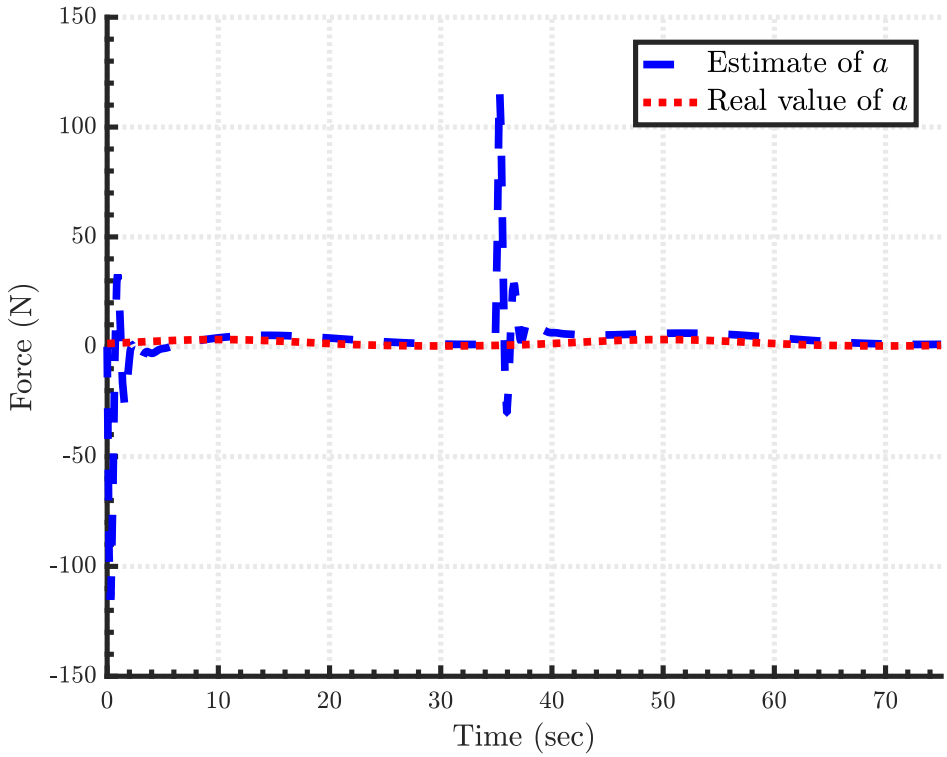

Figure 3.8. Real value of the disturbance term a and its estimate for Case 1

Change of the force input to the crane trolley over time is shown in Figure 3.9. It can be seen that at peak values the force goes up to about 30 kN of magnitude really fast. That is not desirable in a real application. Two of the possible ways to overcome this problem is; trying to optimize the control gains and/or feeding the controller output to a low-pass filter to filter out those quick and erratic changes in force magnitude. Otherwise the force values seem to have an order of magnitude below 10^3 N which is achievable.

(iii) *Case 2: Time varying in-domain and boundary disturbance without drag (air) :* In this case, the disturbance is changed slightly as the boundary disturbance is now taken as a scaled up version of the in-domain disturbance value at $y = l$. The scaling factor is chosen as 25. All other parameters are the same as Case 1. Figures 3.10 to 3.12 show the resulting payload velocity, disturbance and input force values and their estimations.

Comparing Figures 3.7 and 3.10, one can see that the payload velocity has a more visible oscillation about reference velocities. This is expected as the boundary disturbance scaling is relatively high and this makes it harder to be canceled since

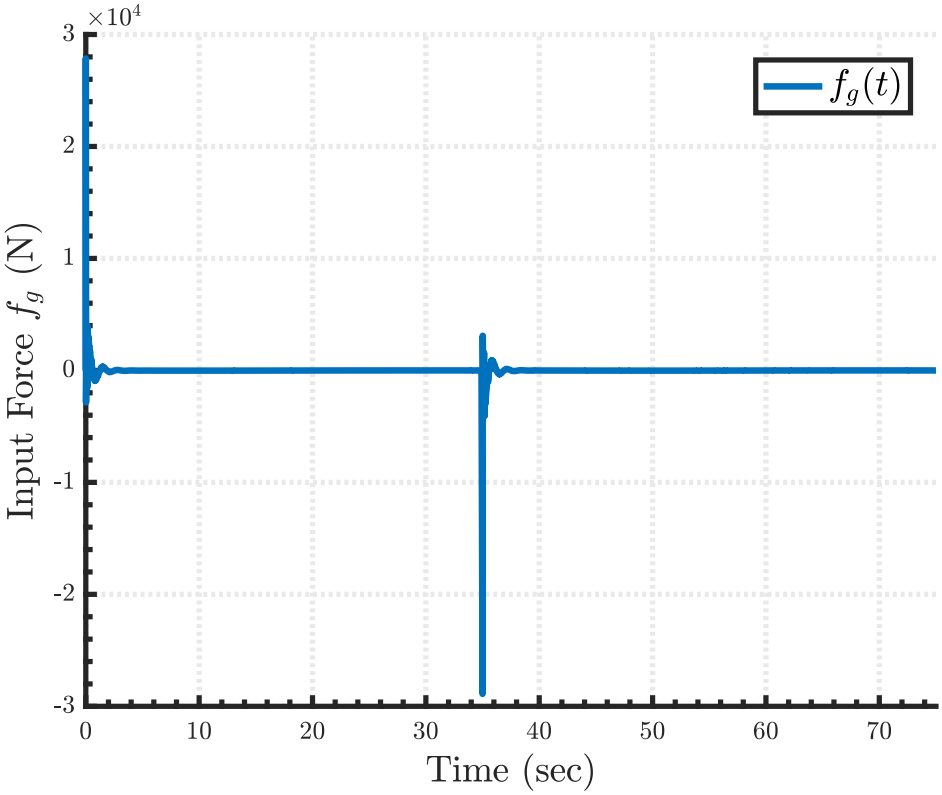

Figure 3.9. Input force $f_g(t)$ for Case 1

the observer doesn't assume a time varying disturbance. Still, the oscillations about the reference velocity has a magnitude about $\sim$ 0.035 m/s. Compared to the 0.78 m/s deviation in open-loop case, this is a satisfying result. This corresponds to a decrease of about 95% in sway speed.

Disturbance term $a(t)$ and its estimate $\hat{a}(t)$ are shown in Figure 3.11. It can be seen that the phase shift observed in Case 1 is still there but also a relatively large bias error exists in the estimation. It is not clear why this is the case but one possible reason might be the constant tracking error present in $w_t(1,t)$ due to the time varying external effects.

(iv) *Case 3: Time varying in-domain and boundary disturbances with drag (air) :* In this case, additional to the previous cases, the drag effect caused by the motion of the cable is added. The implementation of this effect is straightforward. Previously, the external force due to the external flow was being calculated as

$$F^j_{drag} = \frac{1}{2} C_d \rho_f \pi r u_w^2(y_j, t_i) dy \tag{3.42}$$

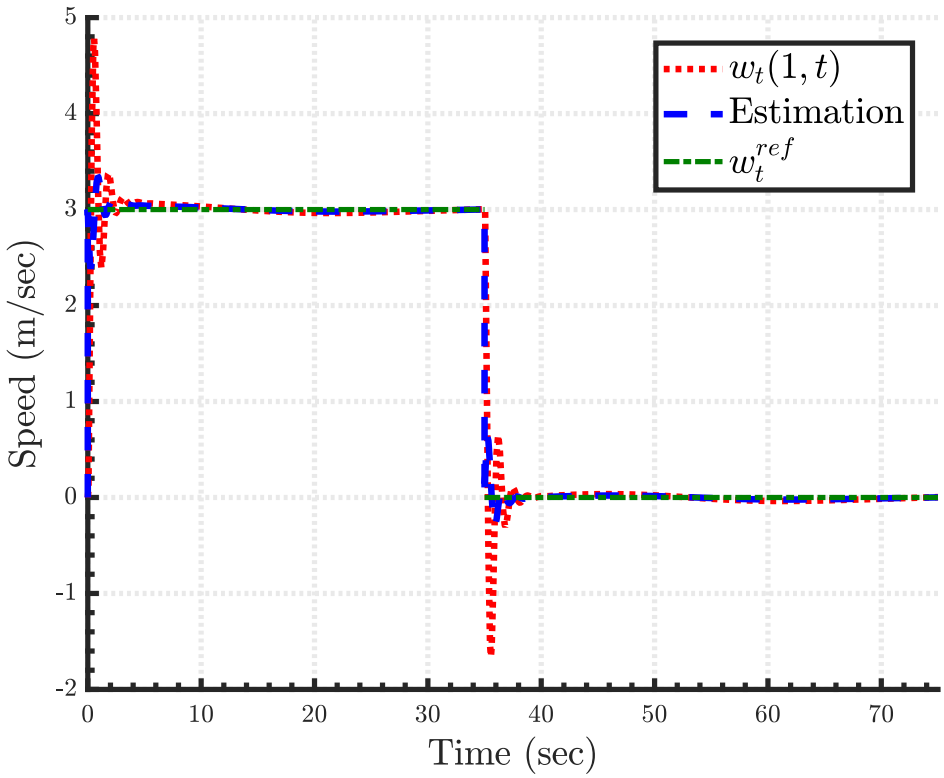

Figure 3.10. Horizontal velocity of the payload and its estimation for Case 2

However, the drag force can be defined as the result of relative motion of an object to the fluid medium it is in. Therefore, for this case, the drag force is calculated as follows.

$$F_{drag}^{j} = \frac{1}{2} C_d \rho_f \pi r \left(u_w(y_j, t_i) - w_t(y_j, t_i)\right)^2 dy \tag{3.43}$$

Figures 3.13 to 3.15 show the resulting payload velocity, disturbance, and input force and their estimations for this case. It can be seen on Figure 3.13 that reference tracking is accomplished with drag effect as well. The sway about reference values in this case is ~ 0.037 m/s. Similar to the previous case, this is considered a success when compared to the open-loop result.

The disturbance term $a(t)$ and $\hat{a}(t)$ are presented in Figure 3.14. There is a visible shift in the mean value of both the real disturbance and the estimation. This is probably due to the overall decrease in the speed of the crane cable. Since wind speed and the cable speed act opposite to each other, when the crane moves in positive direction it negates the effect of the wind speed to some degree. At

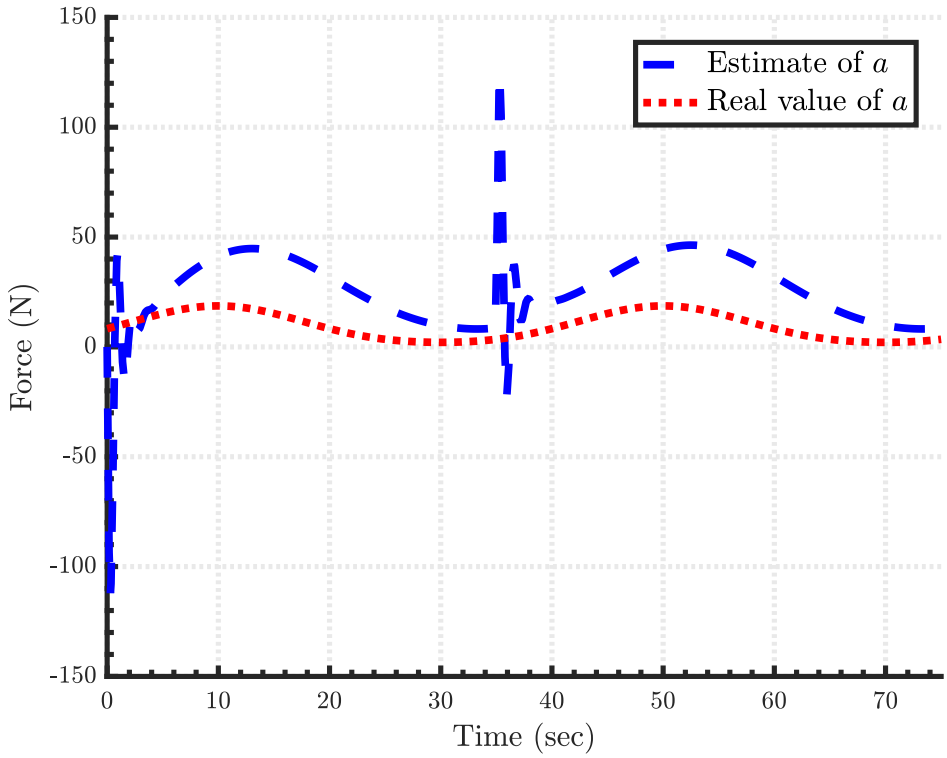

Figure 3.11. Real value of the disturbance term a and its estimate for Case 2

$t = 35$ s however, the reference speed value is set to 0 m/s so it results in an overall decrease in crane cable speed and an increase in net drag force.

(v) *Case 4: Time varying in-domain disturbance without boundary disturbance or drag (water) :* Cases 4, 5, and 6 are exact replicas of Cases 1, 2, and 3 respectively except the medium is changed with water. Therefore the only parameters that are changed are the fluid properties and the drag coefficient C_D. What is expected to be seen in these cases is that due to the increased density and viscosity of the medium, same flow distribution will result in a larger external force. This in turn should result in a faster varying disturbance since the separation between the highest and lowest magnitudes of the disturbing force is much larger although the frequency of the disturbance is the same.

Figures 3.16 to 3.18 show the payload velocity, disturbance, the input force, and their estimations. It can be seen on Figure 3.16 that the controller really struggles in this case. It is observed during simulations that even with water, higher control gains show promising results. However, setting the gains too high results in numerical instability of the simulations. With the current settings no successful combination of gain values have been found. Some of the more

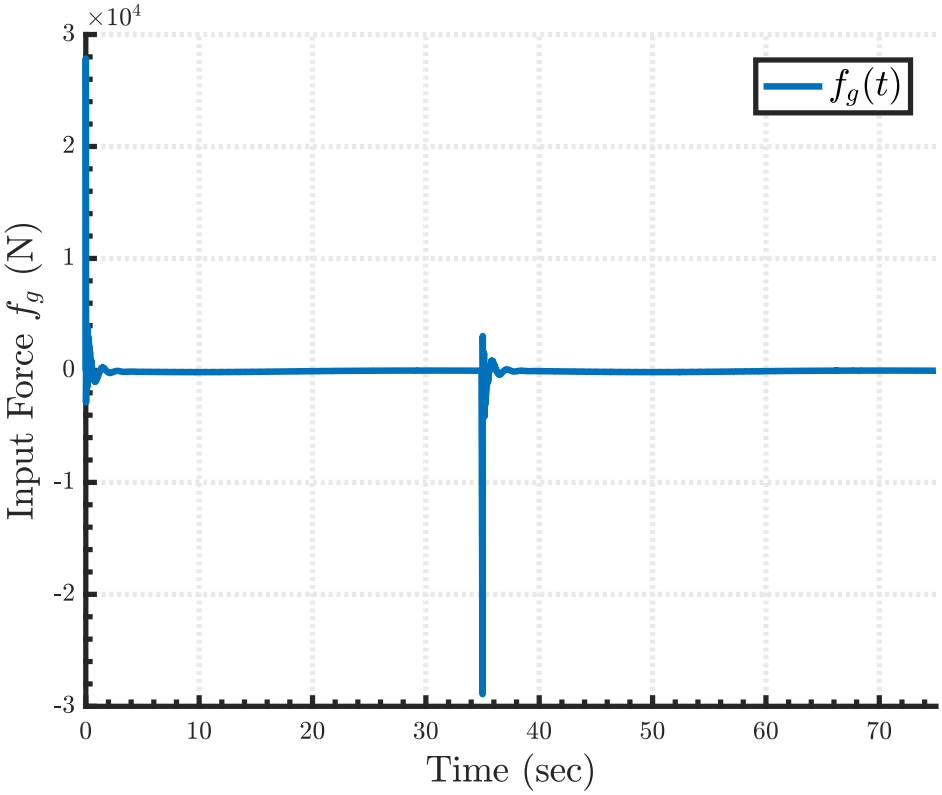

Figure 3.12. Input force $f_g(t)$ for Case 2

promising results either become numerically unstable over time or take too long to converge to the reference values.

(vi) *Case 5: Time varying in-domain and boundary disturbances without drag (water) :* In this case, similar to Case 2, the boundary disturbance scaling factor is taken as 25. Therefore the boundary disturbance term $a_b(t)$ is calculated as

$$\nu_{payload}(t_i) = 25\nu_{cable}(l, t_i) \tag{3.44}$$

Figures 3.19 to 3.21 show the payload velocity, disturbance, the input force, and their estimations. It can be seen from the figures that similar problems to the Case 4 exists for this case as well. This is expected since the only difference is that the disturbance at the payload boundary is amplified.

(vii) *Case 6: Time varying in-domain and boundary disturbances with drag (water) :* In this case the drag force caused by the motion of the system is considered. Similar to Case 3, the external force is calculated using Equation 3.43. Figures 3.22 to 3.24 show the payload velocity, disturbance, input force and their estimates. It

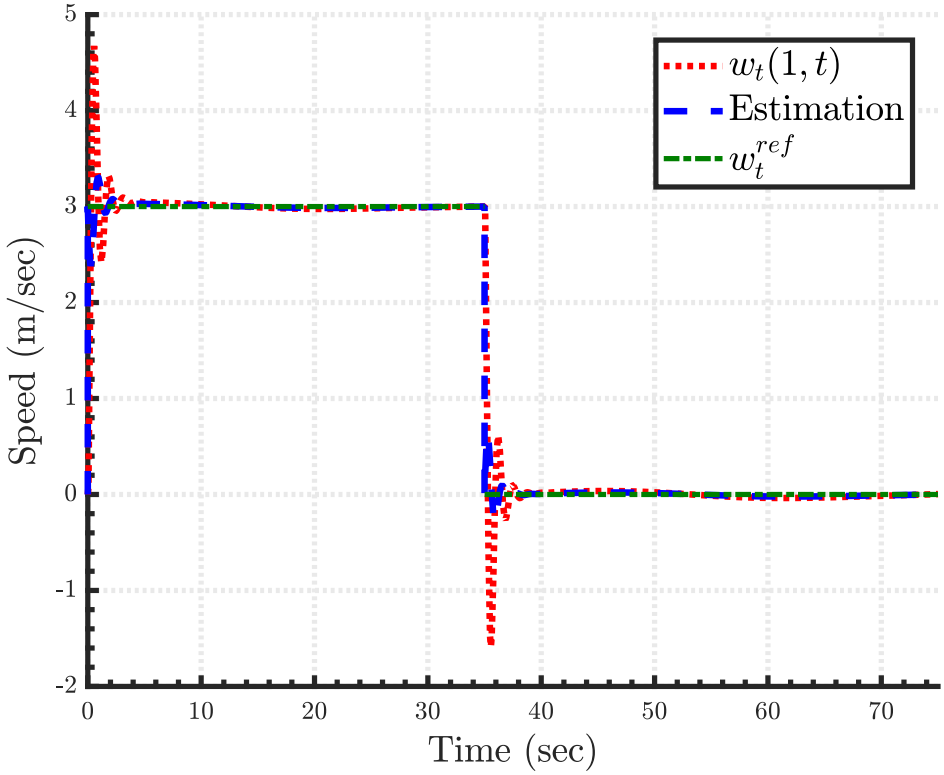

Figure 3.13. Horizontal velocity of the payload and its estimation for Case 3

can be seen that the drag effect actually helps reduce the erratic swaying. However, still the time variance of the external effect is too much for the controller to handle.

(viii) *Case 7: Constant in-domain and boundary disturbances without drag (water) :* This case is studied to show that the convergence problems actually arise from the time varying effect not from the magnitude of the disturbance. The applied flow speed is set to a constant value for this case. Maximum flow speed which was previously calculated as $u_{w,max}(t) = 10 + 5\sin(0.05\pi t)$ is now set to $u_{w,max} = 10$ m/s. Again, all other parameters are the same as the ones before and the drag caused my system motion is not considered. Figures 3.25 to 3.27 show the payload velocity, disturbance, input force and their estimates. As predicted by the results of Chapter 2, the controller achieves exponential convergence with constant external effects.

(ix) *Case 8: Constant in-domain and boundary disturbances with drag (water) :* This case again considers constant flow speed similar to Case 7. However this case also considers the drag force caused by crane motion. Figures 3.28 to 3.30 show

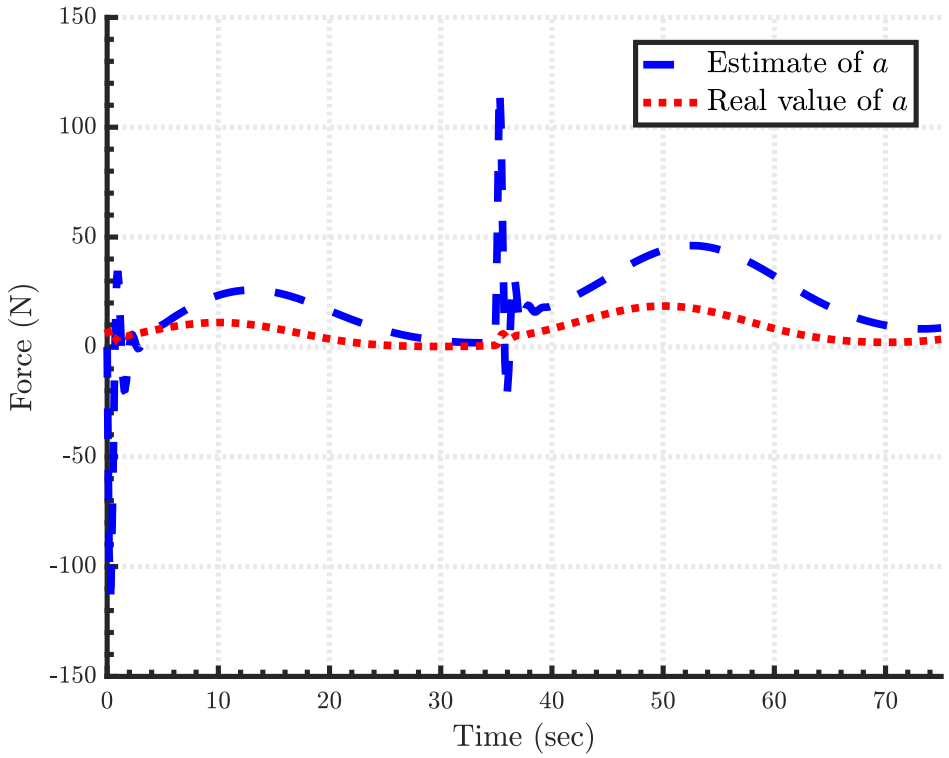

Figure 3.14. Real value of the disturbance term a and its estimate for Case 3

the payload velocity, disturbance, input force and their estimations. As might be expected, the additional drag effect highly increases the convergence time. In fact, to show that the system actually converges to the reference speed, the simulation time has been increased to 200 seconds. It can be seen from Figure 3.28 that the payload velocity tends to the reference value but it does so relatively slowly. This behavior resembles an over-damped response and, again, increasing the control gains can probably solve this issue.

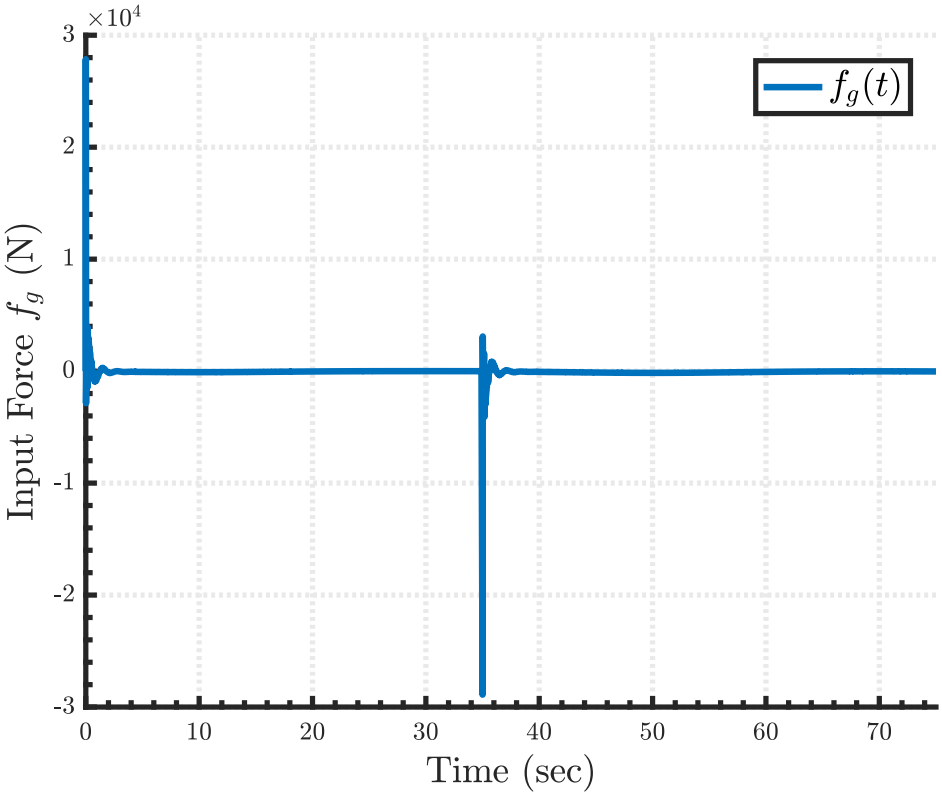

Figure 3.15. Input force $f_g(t)$ for Case 3

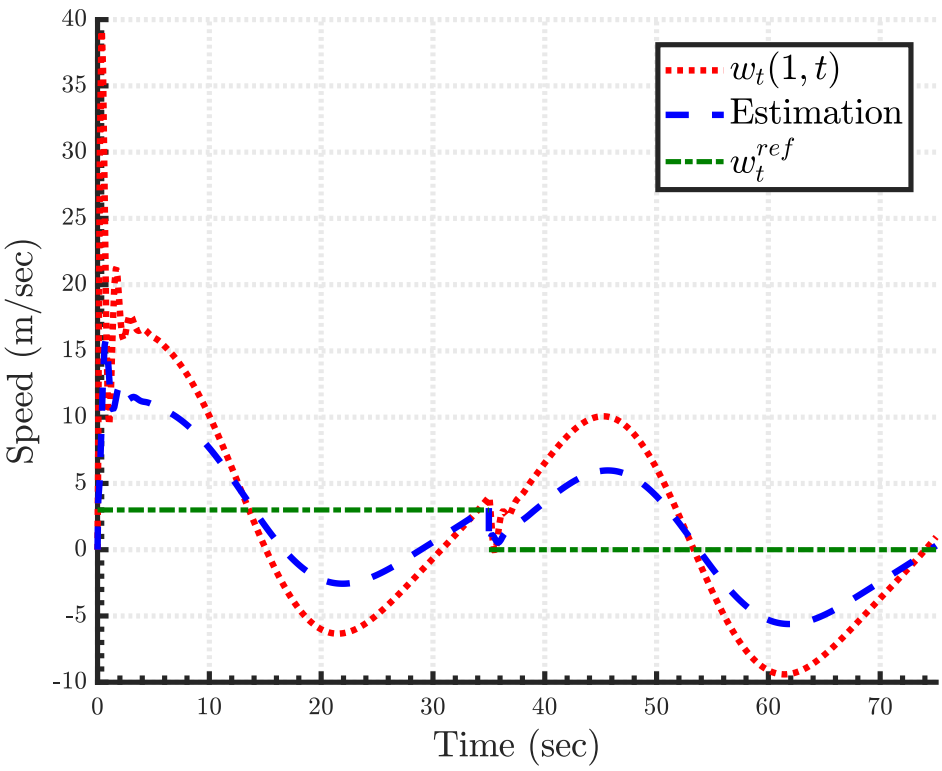

Figure 3.16. Horizontal velocity of the payload and its estimation for Case 4

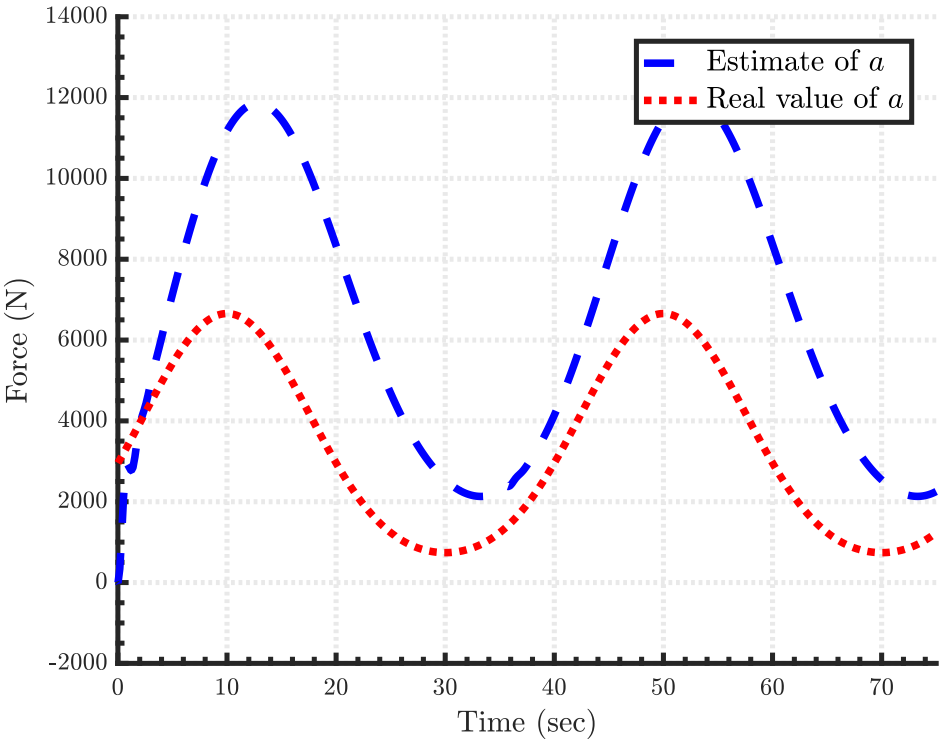

Figure 3.17. Real value of the disturbance term a and its estimate for Case 4

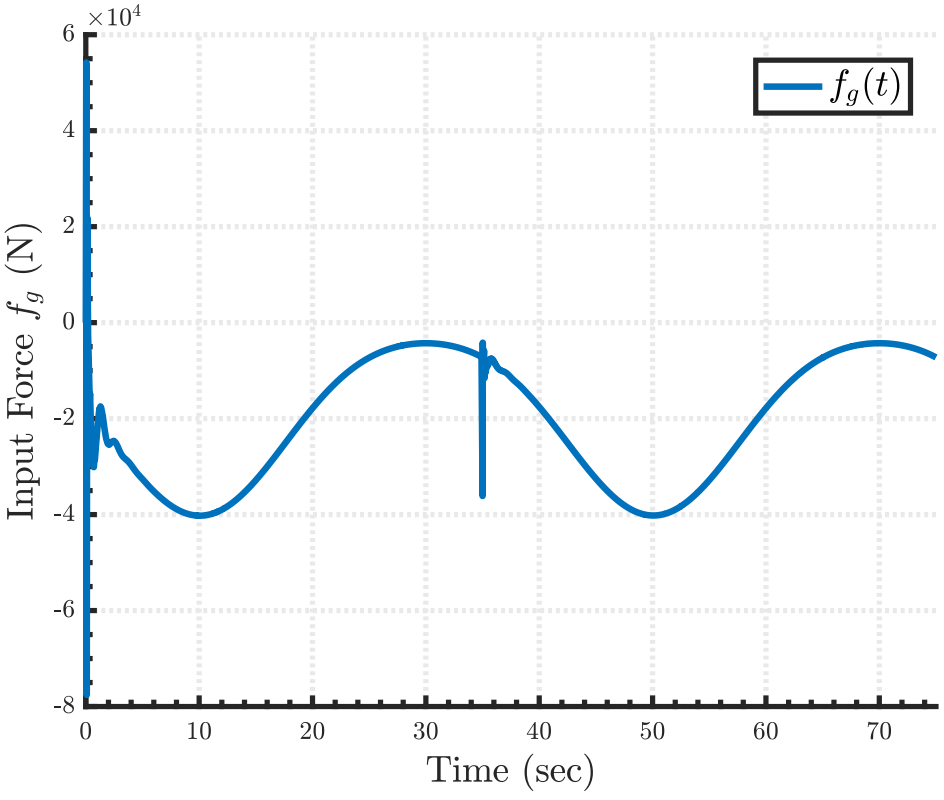

Figure 3.18. Input force $f_g(t)$ for Case 4

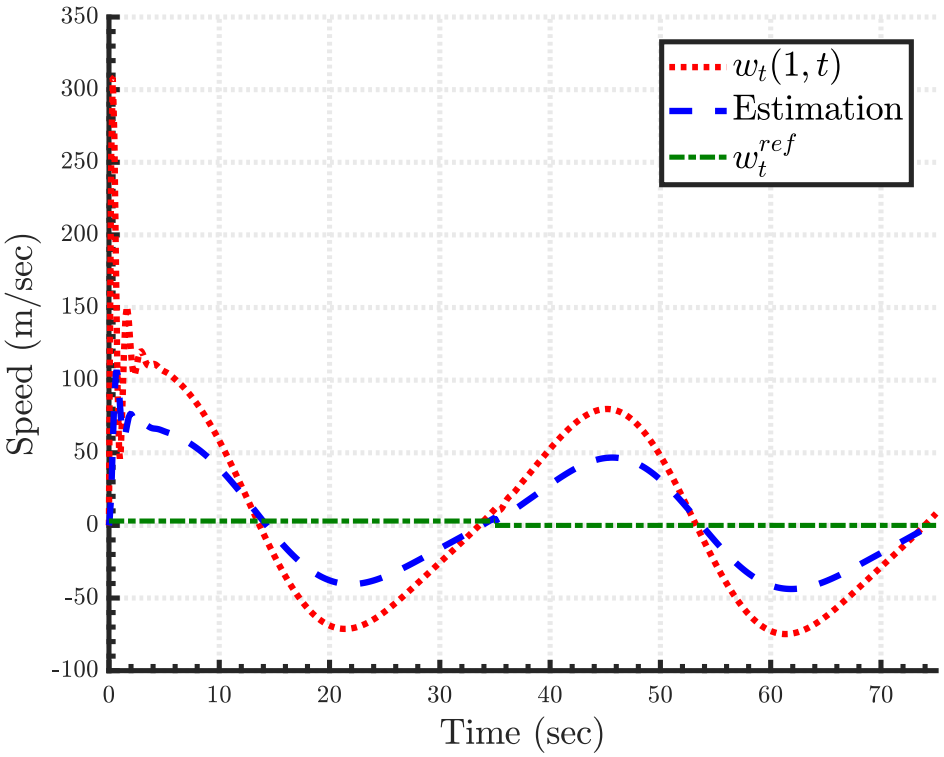

Figure 3.19. Horizontal velocity of the payload and its estimation for Case 5

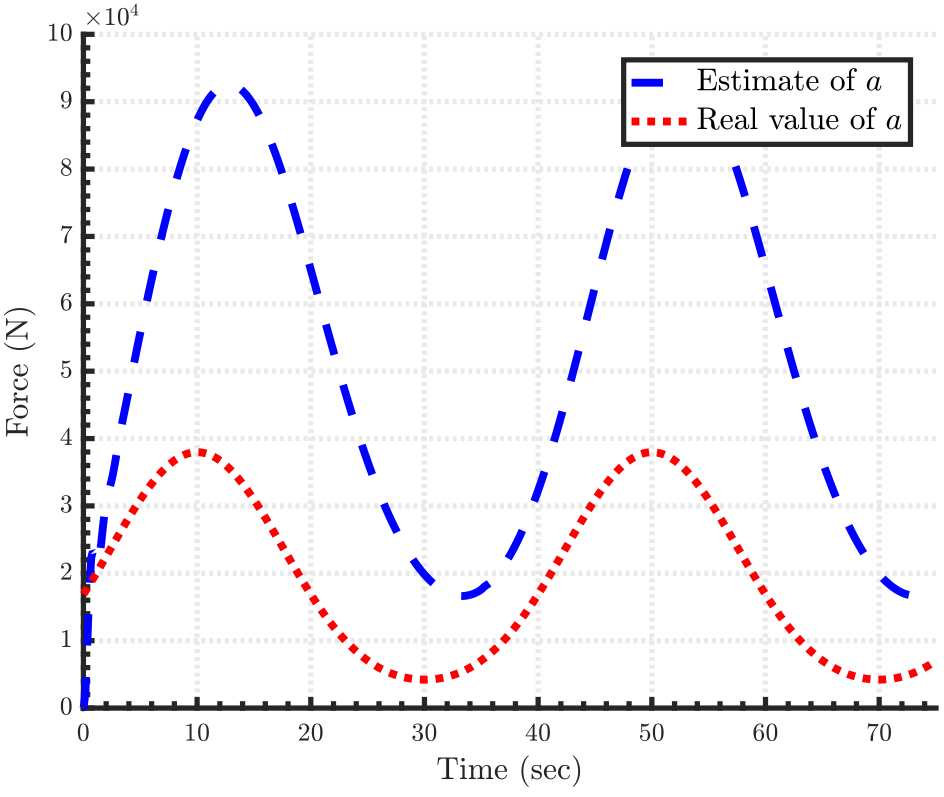

Figure 3.20. Real value of the disturbance term a and its estimate for Case 5

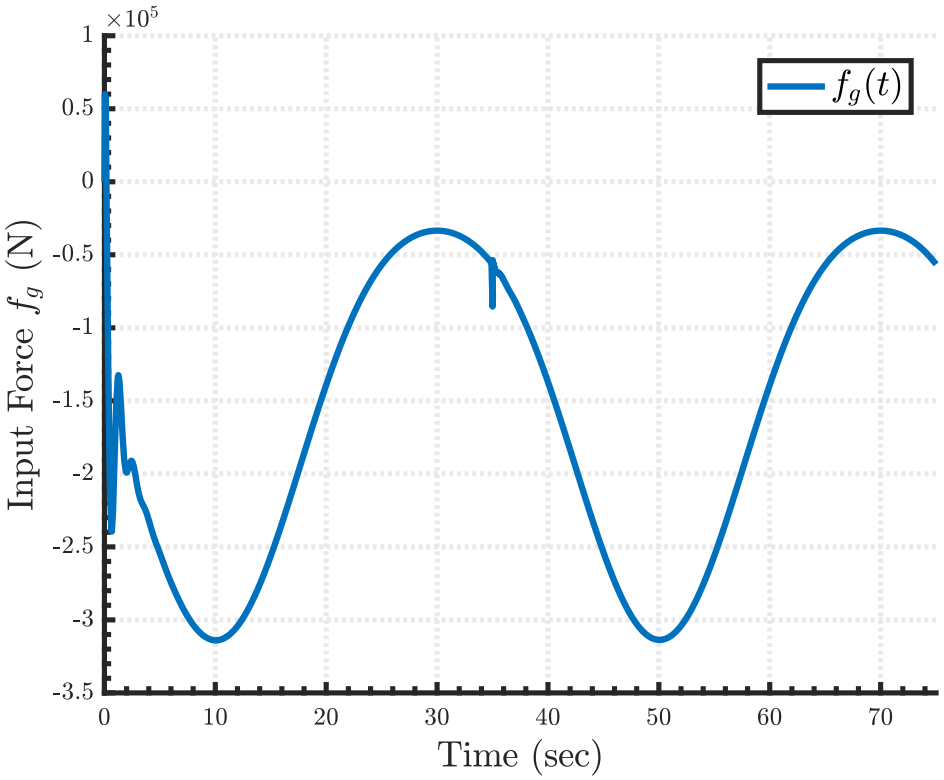

Figure 3.21. Input force $f_g(t)$ for Case 5

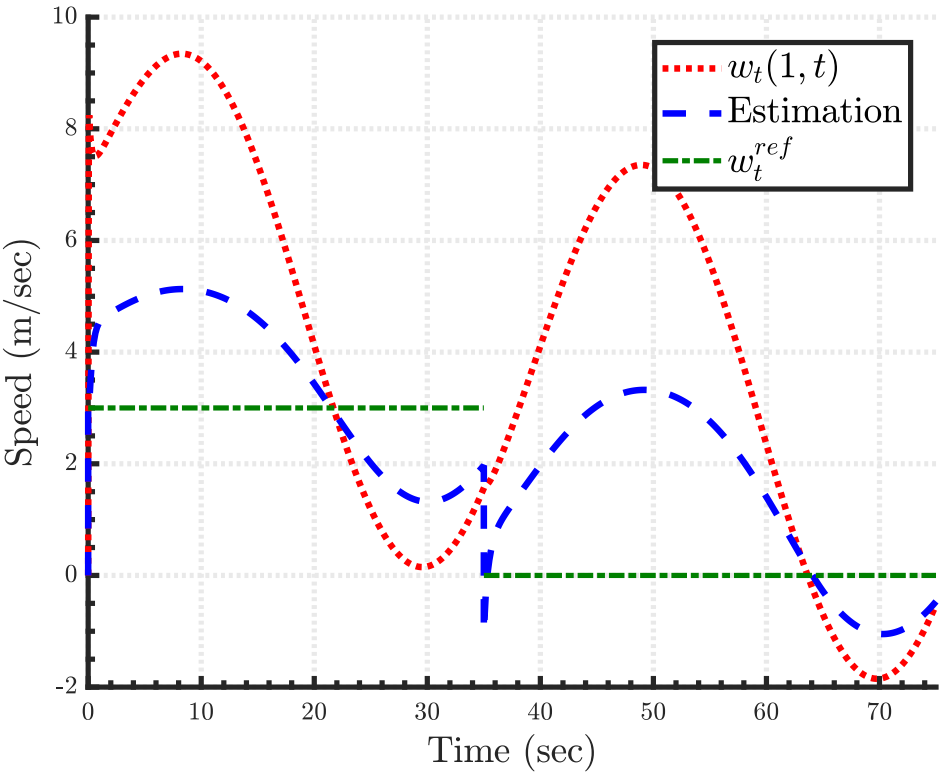

Figure 3.22. Horizontal velocity of the payload and its estimation for Case 6

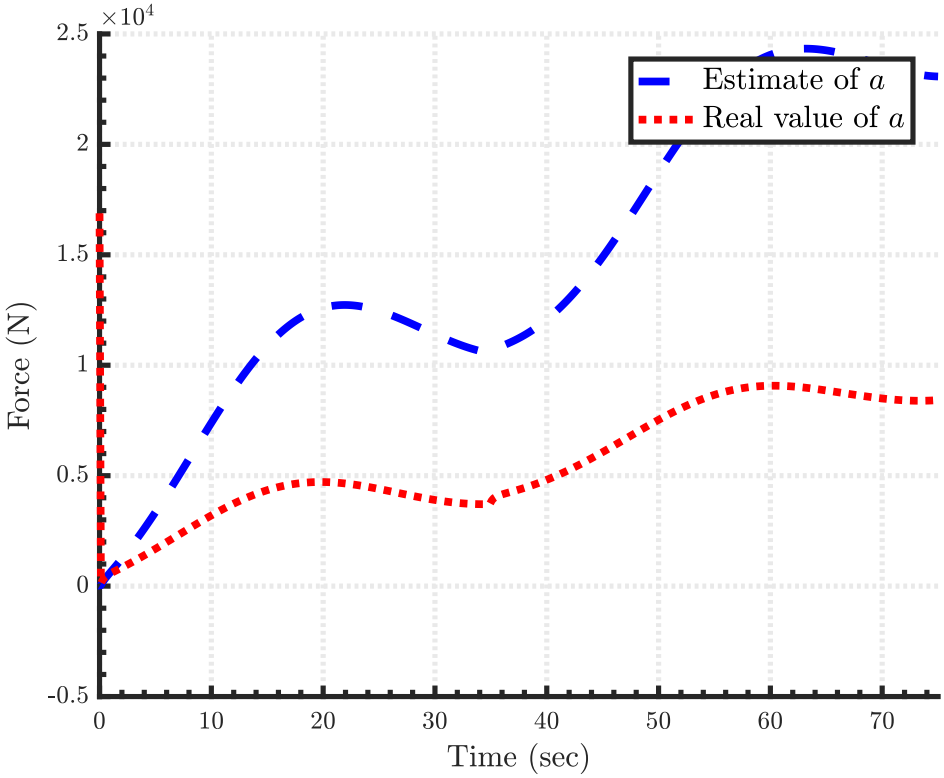

Figure 3.23. Real value of the disturbance term a and its estimate for Case 6

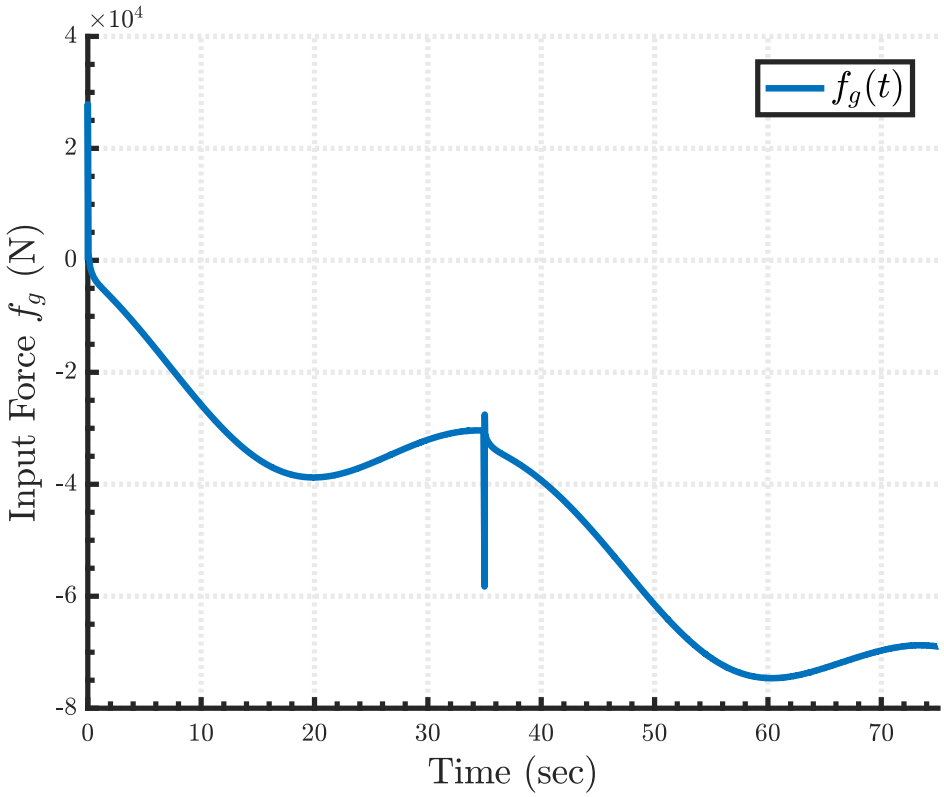

Figure 3.24. Input force $f_g(t)$ for Case 6

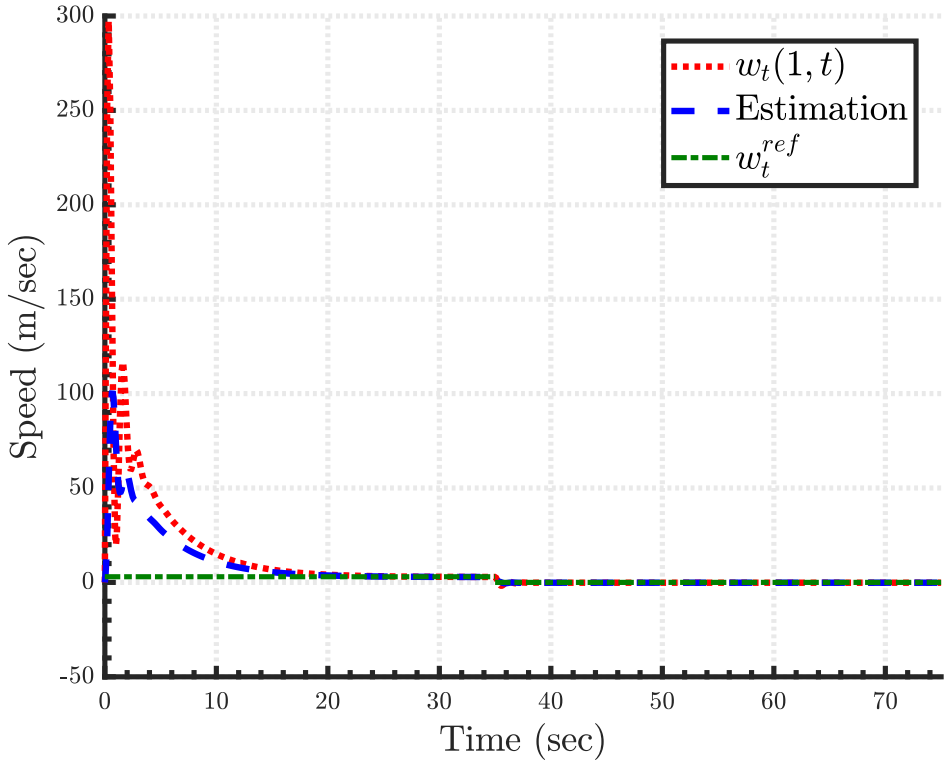

Figure 3.25. Horizontal velocity of the payload and its estimation for Case 7

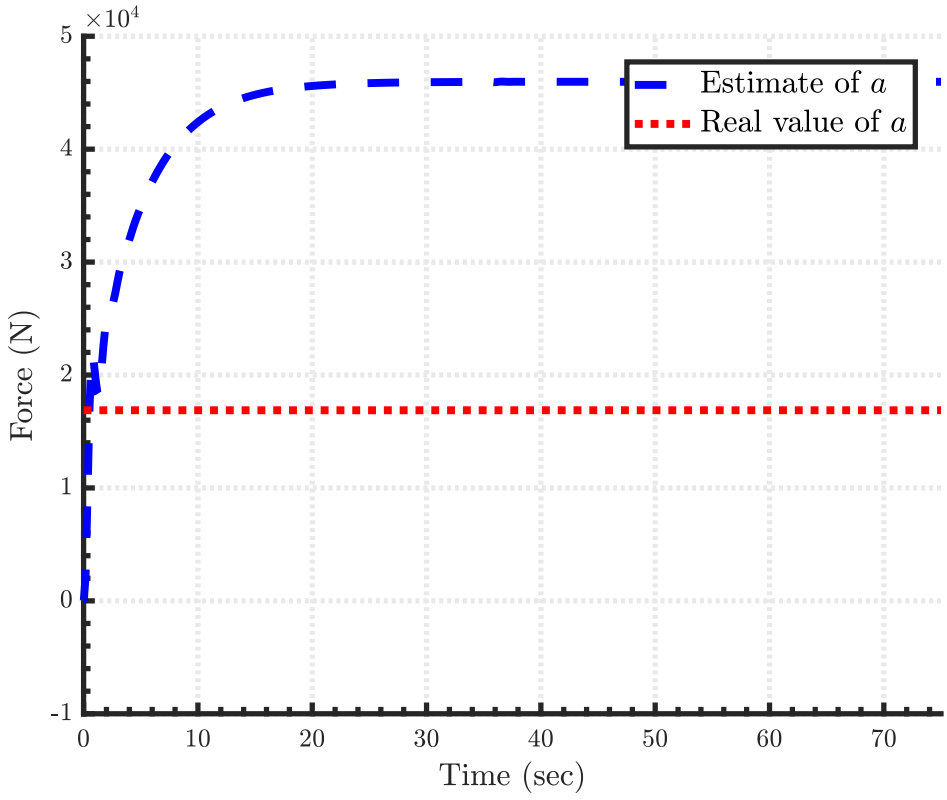

Figure 3.26. Real value of the disturbance term a and its estimate for Case 7

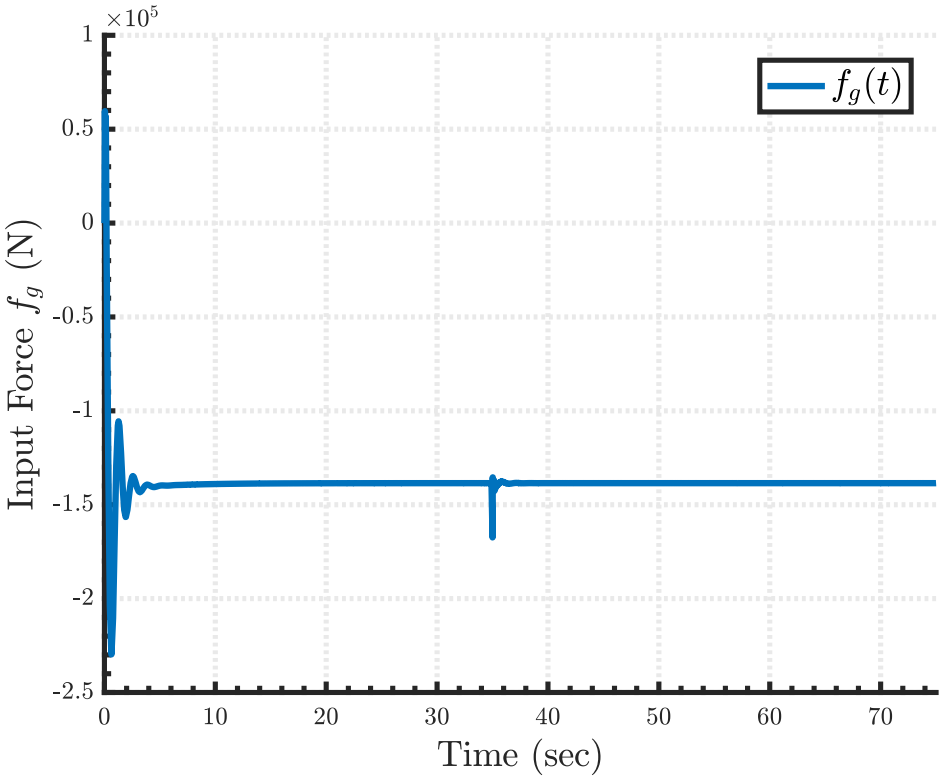

Figure 3.27. Input force $f_g(t)$ for Case 7

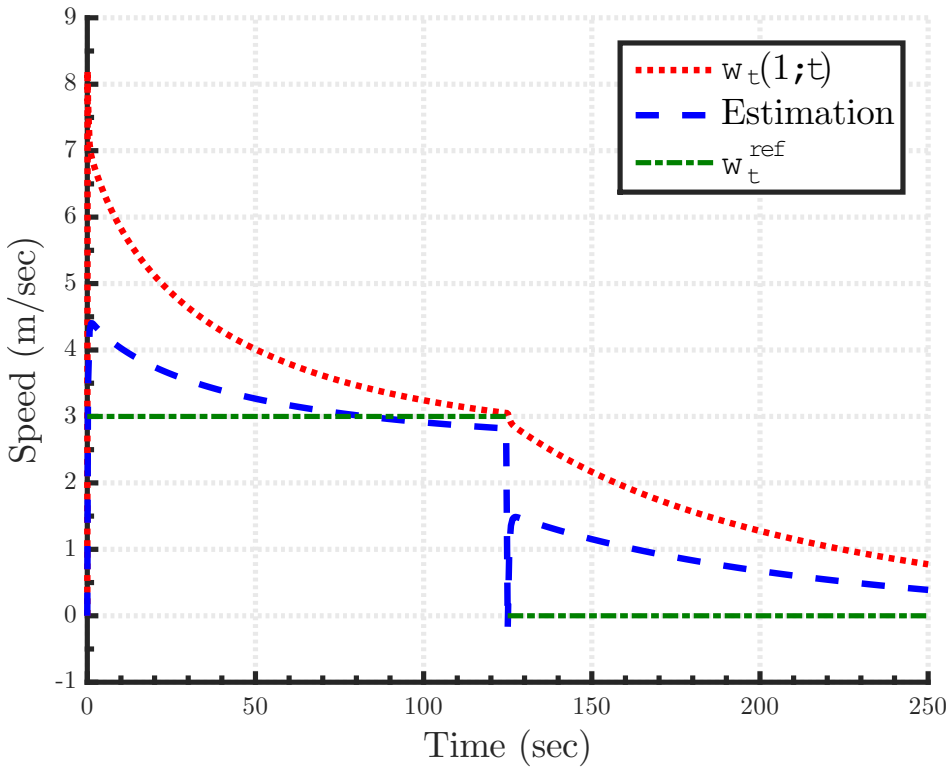

Figure 3.28. Horizontal velocity of the payload and its estimation for Case 8

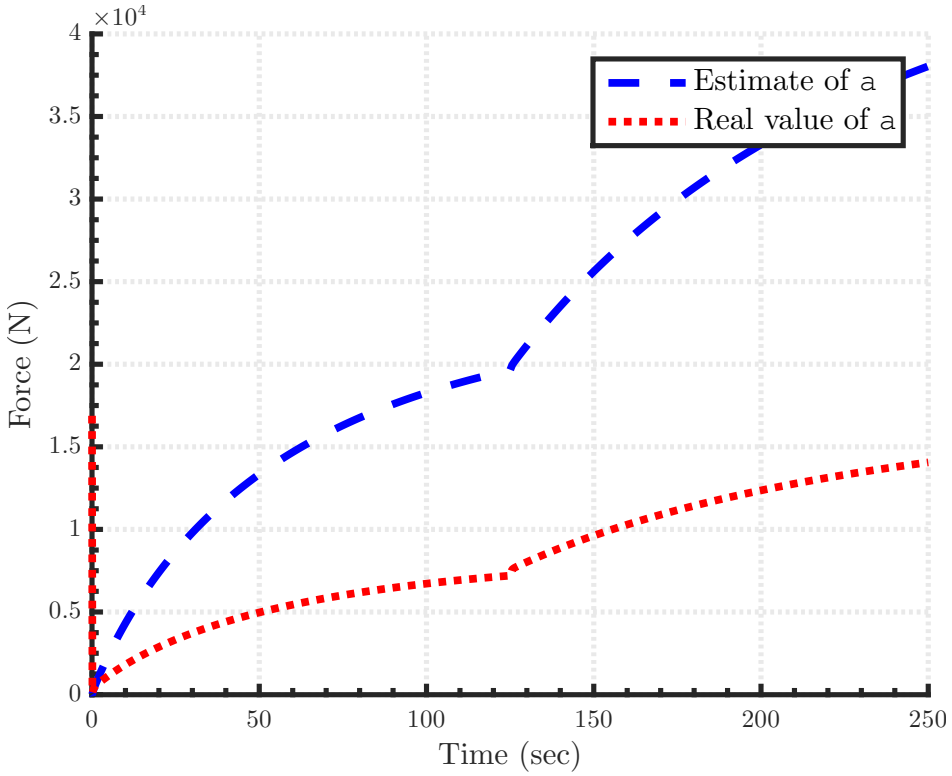

Figure 3.29. Real value of the disturbance term a and its estimate for Case 8

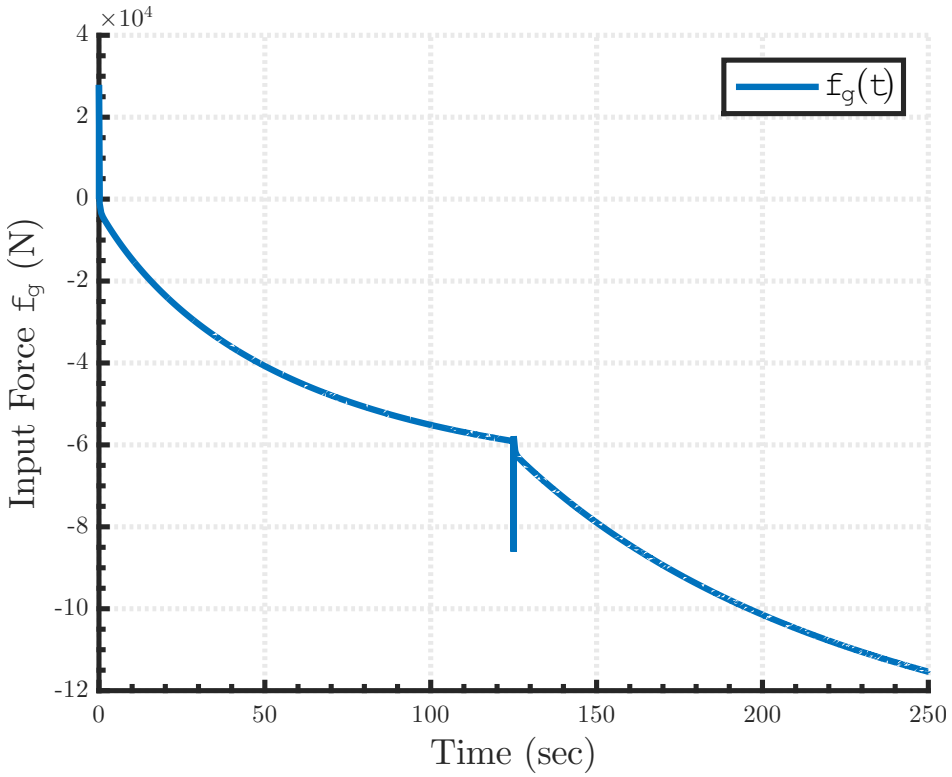

Figure 3.30. Input force $f_g(t)$ for Case 8

4. CONCLUSIONS

The aim of the thesis was to design a regulator for a wave PDE with constant unknown in-domain and boundary disturbances using backstepping boundary control approach where the control input and the measurements are collocated on one boundary and the output signal is on the opposite boundary, then test the controller on a crane model where the disturbance terms vary with time relatively slowly. To this end, the problem is reformulated as control of an ODE with simultaneous input and output delay and constant unknown disturbance. Then an estimator for both the output state and the unknown disturbance effect is designed and a regulator for this estimator is given. The stability and exponential convergence of this controller on a wave PDE with constant disturbances is proven and the performance is shown using numerical simulations, the results of which agree with the mathematical proof. This is the first instance of a backstepping boundary controller being designed for a wave PDE with unknown in-domain and boundary disturbances and limited measurement. Then the controller is applied to an overhead crane model with some necessary transformations.

The model is simulated using numerical methods and the results show that slow variances in external effects (as seen in Cases 1 to 3) can be canceled rather successfully even with the constant disturbance assumption in the controller model. In those cases, the controller has provided about 95% decrease in sway after reference tracking has been accomplished.

However when the fluid that the crane operates in is changed for a denser and more viscous one, larger magnitude of the external effects pose a serious problem. A proper convergence could not be obtained for any of the cases with time varying effects and water as the medium (Cases 4, 5, 6, and 8). However when all the external effects are constant, the controller achieves exponential stability even in water (as seen in Case 7) which is expected since the controller is proven to be exponentially stable with constant disturbance effects.

The inability to achieve convergence in water with time varying effects seems to be largely caused by limitations of the numerical simulations. As the gains are pushed to the limits of numerical stability, the results for those cases get more and more promising. Those limitations and possible future work are discussed in Section 4.1.

4.1. Limitations of the Study and Future Work

One of the main limitations of this study has been the numerical stability of the simulations, especially for the crane model. Although, as stated earlier, the Crank-Nicolson method is shown to be unconditionally stable for the types of PDEs this thesis deals with, the control/observer scheme requires numerous time integrations of the states. It has been observed that when the simulations are not done with small enough time increments, the control input gets unstable which in turn results in erratic behavior of the system. To avoid this, the time increments were adjusted by trial and error over time and that resulted in total runtime of each simulation to get longer and longer. As a result the number of studied cases are very limited. Many of the future work suggested below expand upon that idea as they require more cases to be studied.

- During trial simulations with simpler cases, it has been observed that observer and controller gains directly affect the convergence behavior of the system. With smaller gains, convergence takes longer but the output resembles that of an over-damped linear system with no overshoot. On the other hand, with relatively higher gains the output converges faster but with more swaying and overshoot. Therefore it seems there is still some room for optimization in the controller through adjustment of the gains. However, as mentioned above, the long run times of the simulations makes it harder to try lots of different values of control gains for each and every case. Hence, as future work, the optimization of the control/observer gains might be studied.
- As discussed in Chapter 1, there are many control schemes developed for different modifications of the system considered in this thesis. The suggested controller needs to be compared with its peers to see advantages and disadvantages of this controller against others.

- Although numerical simulations have their advantages as they are fast, easier to set up and can cover lots of different cases with minimal modifications, at the end of the day, they still assume ideal conditions and have their inaccuracies and limitations. For the controller suggested in this thesis to be used in any real life application it should be tested on a prototype first. Also, since the control unit in a real life application would not be burdened by the simulation of the system, much lower time increments for the input force calculation can be achieved. This might allow higher control gains for more difficult environments like water.
- The control model given in Equation 2.1 is a general wave equation and it can be applied to numerous physical phenomena. Crane application done in this text is just one example of its areas of use. The spectrum of applications for the controller can be broadened to vibrating strings, flexible robot arms, oil drills or any mechanical component that can be approximated with an undamped wave PDE.
- The controller model includes an unknown but constant disturbance effect and the observer estimates the value of it. However, in simulation models time varying disturbances are used since a real life situation where the external effects stay constant is very unlikely. Although it is shown that slowly varying disturbance effects with lower magnitudes can still be mostly canceled, as seen in water simulations, the controller struggles with large magnitude variations in the disturbance. Incorporating time varying disturbance dynamics and drag/damping effects into the controller model would highly increase the performance of the controller.

REFERENCES

1. Hoosier Crane Service Co. Hc 10 ton top running crane and hoist. `https://www.hoosiercrane.com/sites/hoosiercrane/files/styles/photo-page/public/hoosier_crane_10_ton_top_running_crane_and_hoist.png`, 2014, accessed at June 2018.

2. K. Hong and Q. Ngo. Port automation: modeling and control of container cranes. *International Conference on Instrumentation, Control & Automation*, (August 2016):19–26, 2009.

3. K. A. F. Moustafa and A. M. Ebeid. Nonlinear Modeling and Control of Overhead Crane Load Sway. *Journal of Dynamic Systems, Measurement, and Control*, 110 (3):266, 1988. ISSN 00220434. doi: 10.1115/1.3152680.

4. H. Park, D. Chwa, and K.-S. Hong. A feedback linearization control of container cranes: Varying rope length. *International Journal of Control Automation and Systems*, 5(4):379, 2007. ISSN 15986446.

5. G. Corriga, A. Giua, and G. Usai. An implicit gain-scheduling controller for cranes. *IEEE Transactions on Control Systems Technology*, 6(1):15–20, 1998. ISSN 10636536. doi: 10.1109/87.654873.

6. J. H. Yang and K. S. Yang. Adaptive coupling control for overhead crane systems. *Mechatronics*, 17(2-3):143–152, 3 2007. ISSN 09574158. doi: 10.1016/j.mechatronics.2006.08.004.

7. G. Bartolini, A. Pisano, and E. Usai. Second-order sliding-mode control of container cranes. *Automatica*, 38(10):1783–1790, 10 2002. ISSN 00051098. doi: 10.1016/S0005-1098(02)00081-X.

8. Kuo-Kai Shyu, Cheng-Lung Jen, and Li-Jen Shang. Design of sliding-mode controller for anti-swing control of overhead cranes. In *31st Annual Conference of IEEE Industrial Electronics Society, 2005. IECON 2005.*, volume 2005, page 6 pp. IEEE, 2005. ISBN 0-7803-9252-3. doi: 10.1109/IECON.2005.1568895.

9. D. Liu, J. Yi, D. Zhao, and W. Wang. Adaptive sliding mode fuzzy control for a two-dimensional overhead crane. *Mechatronics*, 15(5):505–522, 6 2005. ISSN 09574158. doi: 10.1016/j.mechatronics.2004.11.004.

10. D. Qian, J. Yi, and D. Zhao. Control of Overhead Crane Systems by Combining Sliding Mode with Fuzzy Regulator. *IFAC Proceedings Volumes*, 44(1):9320–9325, 1 2011. ISSN 14746670. doi: 10.3182/20110828-6-IT-1002.01716.

11. Q. H. Ngo, N. P. Nguyen, C. N. Nguyen, T. H. Tran, and K.-S. Hong. Fuzzy sliding mode control of container cranes. *International Journal of Control, Automation and Systems*, 13(2):419–425, 4 2015. ISSN 1598-6446. doi: 10.1007/s12555-014-0150-0.

12. H. Aschemann and D. Schindele. IDA Passivity-Based Trajectory Control of an Overhead Travelling Crane. *IFAC Proceedings Volumes*, 42(16):293–298, 2009. ISSN 14746670. doi: 10.3182/20090909-4-JP-2010.00051.

13. D. Poljak, D. Schindele, F. Antritter, H. Aschemann, and C. Hillermeier. Control of an Overhead Crane with the Controlled Lagrangian Method. *IFAC Proceedings Volumes*, 43(14):131–136, 9 2010. ISSN 14746670. doi: 10.3182/20100901-3-IT-2016.00134.

14. N. Sun, Y. Fang, X. Sun, and Z. Xin. An energy exchanging and dropping-based model-free output feedback crane control method. *Mechatronics*, 23(6):549–558, 9 2013. ISSN 09574158. doi: 10.1016/j.mechatronics.2013.04.010.

15. K. T. Hong, C. D. Huh, and K. S. Hong. Command shaping control for limiting the transients way angle of crane systems. *International Journal of Control Automation and Systems*, 1(1):43–53, 2003. ISSN 15986446.

16. K. L. Sorensen, W. Singhose, and S. Dickerson. A controller enabling precise positioning and sway reduction in bridge and gantry cranes. *Control Engineering Practice*, 15(7):825–837, 7 2007. ISSN 09670661. doi: 10.1016/j.conengprac.2006.03.005.

17. M. J. Maghsoudi, Z. Mohamed, S. Sudin, S. Buyamin, H. I. Jaafar, and S. M. Ahmad. An improved input shaping design for an efficient sway control of a nonlinear 3D overhead crane with friction. *Mechanical Systems and Signal Processing*, 92: 364–378, 2017. ISSN 10961216. doi: 10.1016/j.ymssp.2017.01.036.

18. L. Ramli, Z. Mohamed, and H. I. Jaafar. A neural network-based input shaping for swing suppression of an overhead crane under payload hoisting and mass variations. *Mechanical Systems and Signal Processing*, 107:484–501, 7 2018. ISSN 10961216. doi: 10.1016/j.ymssp.2018.01.029.

19. A. M. Abdullahi, Z. Mohamed, H. Selamat, H. R. Pota, M. S. Zainal Abidin, F. S. Ismail, and A. Haruna. Adaptive output-based command shaping for sway control of a 3D overhead crane with payload hoisting and wind disturbance. *Mechanical Systems and Signal Processing*, 98:157–172, 2018. ISSN 10961216. doi: 10.1016/j.ymssp.2017.04.034.

20. B. D'Andréa-Novel, F. Boustany, F. Conrad, and B. P. Rao. Feedback stabilization of a hybrid PDE-ODE system: Application to an overhead crane. *Mathematics of Control, Signals, and Systems*, 7(1):1–22, 3 1994. ISSN 0932-4194. doi: 10.1007/BF01211483.

21. C. D. Rahn, F. Zhang, S. Joshi, and D. M. Dawson. Asymptotically Stabilizing Angle Feedback for a Flexible Cable Gantry Crane. *Journal of Dynamic Systems, Measurement, and Control*, 121(3):563–566, 1999. ISSN 00220434. doi: 10.1115/1.2802516.

22. C.-S. Kim and K.-S. Hong. Boundary control of container cranes from the perspective of controlling an axially moving string system. *International Journal of Control, Automation and Systems*, 7(3):437–445, 6 2009. ISSN 1598-6446. doi: 10.1007/s12555-009-0313-6.

23. W. He and S. S. Ge. Cooperative control of a nonuniform gantry crane with constrained tension. *Automatica*, 66:146–154, 4 2016. ISSN 00051098. doi: 10.1016/j.automatica.2015.12.026.

24. B. Saldivar, S. Mondié, J. J. Loiseau, and V. Rasvan. Stick-slip oscillations in oillwell drilstrings: Distributed parameter and neutral type retarded model approaches. In *IFAC Proceedings Volumes (IFAC-PapersOnline)*, volume 18, pages 284–289, Milano (Italy), 2011. IFAC World Congress. ISBN 9783902661937. doi: 10.3182/20110828-6-IT-1002.00084.

25. H. I. Basturk. Observer-Based Boundary Control Design for the Suppression of Stick–Slip Oscillations in Drilling Systems With Only Surface Measurements. *Journal of Dynamic Systems, Measurement, and Control*, 139(10):104501, 6 2017. ISSN 0022-0434. doi: 10.1115/1.4036549.

26. S.-R. Oh, K. K. Mankala, S. K. Agrawal, and J. S. Albus. Dynamic Modeling and Robust Controller Design of a Two-Stage Parallel Cable Robot. *IEEE Transactions On Control Systems Technology*, 19(1):208–220, 2011.

27. W. He and S. S. Ge. Vibration Control of a Flexible String With Both Boundary Input and Output Constraints. *IEEE Transactions on Control Systems Technology*, 23(4):1245–1254, 7 2015. ISSN 1063-6536. doi: 10.1109/TCST.2014.2362718.

28. V. Komornik and P. Loreti. *Fourier Series in Control Theory*. Springer Monographs in Mathematics. Springer-Verlag, New York, 2005. ISBN 0-387-22383-5. doi: 10.1007/b139040.

29. I. Lasiecka and R. Triggiani. Riccati Equations for Hyperbolic Partial Differential Equations with $L_2(0,T;L_2(\Gamma))$—Dirichlet Boundary Terms. *SIAM Journal on Control and Optimization*, 24(5):884–925, 7 1986. ISSN 0363-0129. doi: 10.1137/0324054.

30. V. Komornik. *Exact controllability and stabilization*. Masson, 1994. ISBN 2-225-84612-X.

31. C. Bardos, G. Lebeau, and J. Rauch. Sharp Sufficient Conditions for the Observation, Control, and Stabilization of Waves from the Boundary. *SIAM Journal on Control and Optimization*, 30(5):1024–1065, 9 1992. ISSN 0363-0129. doi: 10.1137/0330055.

32. G. C. Gorain. Boundary stabilization of nonlinear vibrations of a flexible structure in a bounded domain in R^n. *Journal of Mathematical Analysis and Applications*, 319(2):635–650, 7 2006. ISSN 0022247X. doi: 10.1016/j.jmaa.2005.06.031.

33. V. Komornik. Rapid Boundary Stabilization of Linear Distributed Systems. *SIAM Journal on Control and Optimization*, 35(5):1591–1613, 9 1997. ISSN 0363-0129. doi: 10.1137/S0363012996301609.

34. D. Boskovic, M. Krstic, and Weijiu Liu. Boundary control of an unstable heat equation via measurement of domain-averaged temperature. *IEEE Transactions on Automatic Control*, 46(12):2022–2028, 2001. ISSN 00189286. doi: 10.1109/9.975513.

35. M. Krstic, B. Z. Guo, A. Balogh, and A. Smyshlyaev. Output-feedback stabilization of an unstable wave equation. *Automatica*, 44(1):63–74, 1 2008. ISSN 00051098. doi: 10.1016/j.automatica.2007.05.012.

36. A. Smyshlyaev and M. Krstic. Boundary control of an anti-stable wave equation with anti-damping on the uncontrolled boundary. *Systems & Control Letters*, 58 (8):617–623, 8 2009. ISSN 01676911. doi: 10.1016/j.sysconle.2009.04.005.

37. M. Krstic. Compensating a string PDE in the actuation or sensing path of an unstable ODE. In *Proceedings of the American Control Conference*, pages 4097–4102, 2009. ISBN 9781424445240. doi: 10.1109/ACC.2009.5159876.

38. M. Krstic. Adaptive control of an anti-stablewave pde. *Dynamics of Continuous, Discrete and Impulsive Systems Series A: Mathematical Analysis*, 17(6):853–882, 2010.

39. D. Bresch-Pietri and M. Krstic. Output-feedback adaptive control of a wave PDE with boundary anti-damping. *Automatica*, 50(5):1407–1415, 5 2014. ISSN 00051098. doi: 10.1016/j.automatica.2014.02.040.

40. P. Bernard and M. Krstic. Adaptive output-feedback stabilization of non-local hyperbolic PDEs. *Automatica*, 50(10):2692–2699, 10 2014. ISSN 00051098. doi: 10.1016/j.automatica.2014.09.001.

41. W. Guo, Z. C. Shao, and M. Krstic. Adaptive rejection of harmonic disturbance anticollocated with control in 1D wave equation. *Automatica*, 79:17–26, 2017. ISSN 00051098. doi: 10.1016/j.automatica.2017.01.034.

42. W. He and S. S. Ge. Robust Adaptive Boundary Control of a Vibrating String Under Unknown Time-Varying Disturbance. *IEEE Transactions on Control Systems Technology*, 20(1):48–58, 2011. ISSN 1063-6536. doi: 10.1109/TCST.2010.2099230.

43. D. Bresch-Pietri and M. Krstic. Adaptive output feedback for oil drilling stick-slip instability modeled by wave PDE with anti-damped dynamic boundary. In *Proceedings of the American Control Conference*, pages 386–391, 2014. ISBN 9781479932726. doi: 10.1109/ACC.2014.6858642.

44. M. Krstic and A. Smyshlyaev. *Boundary control of PDEs : a course on backstepping designs*. Society for Industrial and Applied Mathematics, 2008. ISBN 0898716500.

45. C. Sagert. *Infinite-dimensional approaches for the suppression of stick-slip vibrations in oil well drilling*. PhD thesis, University of Stuttgart, 2012.

46. B. R. Munson, D. F. Young, T. H. Okiishi, and W. W. Huebsch. *Fundamentals of Fluid Mechanics*. Wiley, 6 edition, 2009. ISBN 0470262842, 9780470262849.

47. Naval Civil Engineering Laboratory. A Survey of Available Data on the Normal Drag Coefficients of Cables Subjected to Cross-Flow. Technical report, Civil Engineering Laboratory, Naval Construction Battalion Center, Port Hueneme, California, 1977.

48. J. Li and Yi-Tung Chen. *Computational Partial Differential Equations Using MATLAB*. Chapman and Hall/CRC, 10 2008. ISBN 9781420089059. doi: 10.1201/9781420089059.

49. Stormfax Inc. Beaufort Wind Scale. `http://www.stormfax.com/beaufort.htm`, 2018, accessed at May 2018.